The Geometry of Nutrient-space Based Life-history Trade-offs: Sex-Specific Effects of Macronutrient Intake on the Trade-off Between Encapsulation Ability and Reproductive Effort in Decorated Crickets

James Rapkin¹, Kim Jensen^{1,2},C. Ruth Archer¹, Clarissa M. House^{1,5}, Scott K. Sakaluk³,

Enrique del Castillo⁴ and John Hunt^{1,5,6}

- 1. Centre for Ecology and Conservation, College of Life and Environmental Sciences, University of Exeter, Tremough Campus, Penryn, TR10 9EZ, United Kingdom.
- 2. Department of Bioscience, Terrestrial Ecology, Aarhus University, Vejlsøvej 25, 8600 Silkeborg, Denmark.
- 3. School of Biological Sciences, Illinois State University, Normal, Illinois 61790-4120, United States of America.
- 4. Department of Industrial Engineering and Department of Statistics, 357 Leonhard
 Building, Pennsylvania State University, University Park, Pennsylvania 16802, United
 States of America.
- 5. School of Science and Health, Western Sydney University, Hawkesbury Campus, Locked Bag 1797, Richmond, NSW 2753, Australia.
- 6. E-mail: J.Hunt@westernsydney.edu.au

Running title: Macronutrient intake and life-history trade-offs

Abstract

Life-history theory assumes that traits compete for limited resources resulting in trade-offs. The most commonly manipulated resource in empirical studies is the quantity or quality of diet. Recent studies using the Geometric Framework for nutrition, however, suggest that trade-offs are often regulated by the intake of specific nutrients but a formal approach to identify and quantify the strength of such trade-offs is lacking. We posit that trade-offs occur whenever life-history traits are maximised in different regions of nutrient space, as evidenced by non-overlapping 95% confidence regions of the global maximum for each trait, and large angles (θ) between linear nutritional vectors and Euclidean distances (d) between global maxima. We then examined the effects of protein and carbohydrate intake on the trade-off between reproduction and aspects of immune function in male and female Gryllodes sigillatus. Female encapsulation ability and egg production increased with the intake of both nutrients, whereas male encapsulation ability increased with protein intake but calling effort increased with carbohydrate intake. The trade-offs between traits was therefore larger in males than females, as demonstrated by significant negative correlations between the traits in males, non-overlapping 95% confidence regions and larger estimates of θ and d. Under dietary choice, the sexes had similar regulated intakes but neither optimally regulated nutrient intake for maximal trait expression. We highlight that greater consideration of specific nutrient intake is needed when examining nutrient-space based trade-offs.

Key Words: Dietary Choice, Geometric Framework, *Gryllodes sigillatus*, Immune Function, Reproductive Effort, Trade-offs

Introduction

Life-history traits are often negatively correlated with each other (Reznick 1985; Stearns 1992; Roff 2002). These negative correlations, referred to as life-history trade-offs, form the cornerstone of life-history theory and are central to predicting the optimal life-history of an organism in a given environment (Stearns, 1992; Roff, 2002; Reznick *et al.*, 2000; Roff and Fairbairn, 2007). Phenotypic trade-offs exist because different life-history traits compete for a finite pool of resources, so that the allocation of resources to one trait necessarily means there are fewer resources available to allocate to other traits (Stearns 1992; Roff 2002). In this way, trade-offs have the potential to constrain the evolution of life-history strategies, as both traits involved in the trade-off cannot be simultaneously maximised (Roff and Fairbairn, 2007).

While trade-offs between life-history traits appear taxonomically widespread, positive phenotypic correlations are also commonly found in both laboratory and natural populations (Stearns 1992; Reznick et al. 2000; Roff 2002). One of the most prominent models explaining this variation in the sign of phenotypic correlations between life-history traits is the acquisition-allocation model (more commonly known as the "Y-model") of Van Noordwijk and de Jong (1986). This model (and subsequent extensions) posits that the sign of the covariance between life-history traits depends critically on the relative variances in the acquisition and allocation of resources (Van Noordwijk and de Jong 1986; Roff and Fairbairn 2007). More specifically, if the sum of the variances in resource allocation to the two life-history traits $(\sigma_{\chi 1}^2 + \sigma_{\chi 2}^2)$ exceeds the variance in resource acquisition (σ_T^2) , then a negative covariance between life-history traits will occur, whereas if $\sigma_T^2 > (\sigma_{x1}^2 + \sigma_{x2}^2)$, then a positive covariance will occur (Roff and Fairbairn 2007). In other words, if variation in resource acquisition is much larger than variation in resource allocation, trade-offs may be obscured. Despite the elegance of this theoretical prediction, direct empirical tests have proven challenging due, in part, to the difficulties associated with quantifying resource acquisition (Stearns 1992; Roff 2002; Roff and Fairbairn 2007). Although a number of different measures have been used as proxies for resource acquisition, including body size at a given age (e.g. Dudycha and Lynch 2005) and lipid stores (e.g. Chippindale et al. 1998), a more powerful approach to examine trade-offs in life-history studies is to experimentally alter resource acquisition ability through dietary manipulation (Reznick 1985; Reznick et al.

2000; Roff and Fairbairn 2007). Indeed, empirical studies on a range of animal taxa have shown that manipulating the quantity and/or quality of the available diet can have a profound effect on the trade-off between different life-history traits (e.g. invertebrates: Hunt et al. 2004; fish: Kolluru and Grether 2005; amphibians: Lardner and Loman 2003; reptiles: Brown and Shine 2002; birds: Karell et al. 2007; and mammals: Hill and Kaplan 1999).

Reproduction and immune function are major determinants of fitness and are therefore central to the life-history of most organisms (Reznick 1985; Stearns 1992; Roff 2002). Both processes are energetically demanding and have been shown to trade-off in a range of animal taxa (e.g. invertebrates: Schwenke et al. 2016; fish: Kalbe et al. 2009; amphibians: McCallum and Trauth 2007; reptiles: French et al. 2007; birds: Nordling et al. 1998; mammals: Mills et al. 2009). This energetic requirement of reproduction and immune function suggests that the competitive allocation of limiting resources is likely to be the basis for the trade-off between these traits (Zera and Harshman 2001). Indeed, numerous studies have shown that this trade-off is "facultative", being less pronounced or absent when individuals have ad libitum access to food (e.g. French et al. 2007) or only occurring during energetically taxing reproductive periods (e.g. Adamo et al. 2001). However, the trade-off between reproduction and immune function may also be "obligate" whereby physiological changes that occur during reproduction directly impact immune function or vice versa (e.g. Schuurs and Verheul 1990; Sadd and Siva-Jothy 2006). In such cases, the trade-off between reproduction and immune function should be independent of resource acquisition. To evaluate whether the trade-off between reproduction and immune function is "facultative" or "obligate", therefore, requires having some insight into which resource limits investment in these traits and how that resource(s) is allocated (Zera and Harshman 2001; Schwenke et al. 2016).

It is likely that the sexes will adopt very different strategies when allocating resources to immune function and reproduction. This is because in most sexually reproducing species, males and females possess different optimal reproductive strategies that promotes the evolution of sex differences in the trade-off between reproduction and immune function (Rolff 2002; Zuk and Stoehr 2002; Zuk 2009). Females typically invest heavily in reproduction, producing nutrient-rich eggs and providing more parental care, so that their reproductive success is limited by the number of offspring that can be produced

and reared (Bateman 1948; Trivers 1972). As females can produce more offspring by living longer, they are expected to invest less in current reproduction and more in immune function (Rolff 2002; Zuk and Stoehr 2002; Zuk 2009). In contrast, males typically invest less in reproduction than females and their reproductive success is limited by the number of mates they can fertilize (Bateman 1948; Trivers 1972) which is expected to favour a "live hard, die young" strategy characterised by investing heavily in current reproduction at the expense of immune function and lifespan (Rolff 2002; Zuk and Stoehr 2002; Zuk 2009). This divergence in reproductive strategies is predicted to result in males having a weaker immune system than females and exhibit a stronger trade-off between reproduction and immune function (Rolff 2002; Zuk and Stoehr 2002; Zuk 2009). Mathematical models, however, have shown that this general pattern may not necessarily be favoured under all conditions (Medley 2002; Stoehr and Kokko 2006; Restif and Amos 2010). For example, the above argument assumes that lifespan is more important to female than male fitness and that the primary benefit of an enhanced immune system is increased lifespan but if these assumptions are relaxed it is theoretically possible for this pattern to be reversed in the sexes (Stoehr and Kokko 2006). Empirical studies largely agree with the variability of outcomes highlighted by theoretical models. In birds and mammals, males typically have a reduced immune response relative to females (Poulin 1996; Zuk and McKean 1996; Moore and Wilson 2002), but this pattern is far from clear in arthropods (Sheridan et al. 2000). Far fewer studies have directly compared the trade-off between immunity and reproduction in the sexes and those that exist show a mixture of results, with the trade-off being stronger in males than females in some species (e.g. McNamara et al. 2013) but the reverse pattern (e.g. Moreno et al. 2001; Bathal et al. 2015) or no sex difference (e.g. Fedorka et al. 2004) being observed in others. Clearly more detailed empirical work is needed that directly compares how the sexes allocate resources to reproduction and immune function (Zuk 2009).

A limitation of most life history studies using diet to manipulate resource acquisition, is that typically only a few diets of poorly defined nutritional composition (e.g. "good" versus "bad" diets) are used and diet consumption is rarely measured (e.g. Hunt et al. 2004). This approach makes it difficult (if not impossible) to statistically partition the effects of specific nutrients from energy or to examine how nutrients interact to affect life-history traits. Furthermore, not measuring dietary intake ignores any effects of compensatory

feeding. Compensatory feeding, the ability of an individual to increase consumption to compensate for reduced food quality (Simpson and Raubenheimer 2012), appears widespread in animals (Behmer 2009) and means that it is possible for individuals on poorer quality diets to consume as much energy or nutrients as on a high quality diet.

Compensatory feeding, therefore, has the potential to undermine the use of diet to manipulate resource acquisition in life-history studies. These limitations, however, can be resolved by measuring the precise intake of chemically defined (holidic) diets within the geometric framework for nutrition (Simpson and Raubenheimer 2012).

The geometric framework for nutrition is a state-space modelling approach that examines how an individual solves the problem of balancing the need for multiple nutrients in a complex, multidimensional nutritional environment (Simpson and Raubenheimer 2012). To determine the intake of nutrients that is optimal for a given life-history trait, individuals are constrained to feed on a range of diets of precise nutritional composition. These diets are typically arranged in a geometric array (Figure 1A), being positioned along discrete nutritional rails where the ratio of nutrients is fixed (solid lines, Figure 1A) and on iso-caloric lines across different nutritional rails where the nutrient ratio differs but the total nutritional (i.e. caloric) content of the diets is the same (dashed lines, Figure 1A). Consequently, diets differ in both the ratio of nutrients and overall nutritional content. Individuals are allowed to feed for a given period of time and the consumption of diets (and therefore nutrients) is precisely measured. As individuals are constrained to a single diet in this array, they can only feed along the length of a given nutritional rail (Figure 1B). Lifehistory traits can then be measured, mapped as a third axis on top of the two-dimensional nutrient intake data and response surface methodologies (Lande and Arnold 1983; Box and Draper 1987) can be used to determine the linear and nonlinear effects of nutrient intake on the measured life-history traits (see South et al. 2011). Life-history optima can be formally demonstrated by the presence of significant negative quadratic terms in this analysis and non-parametric thin-plate splines (Green and Silverman 1994) can be used to help visualize these optima by constructing nutritional landscapes (Figure 1C). A separate set of individuals can then be provided with a choice of diets to determine how they actively regulate their intake of nutrients (Simpson and Raubenheimer 2012). Alternate diets are typically provided in pairs differing in both the nutrient ratio and overall energy content: in the example provided (red circles, Figure 1A), diets vary in nutrient ratio (i.e. 1:8 or 8:1) and

total energetic content (i.e. 40% or 80%) and diet pairs can be created by matching diets across nutritional rails and caloric content (e.g. diets 1 versus 3, 1 versus 4, 2 versus 3 and 2 versus 4). The consumption of each diet in these pairs is again precisely measured over a given time period to determine the regulated intake point, defined as the point in nutrient space that individuals actively defend when given choice (Simpson and Raubenheimer 2012), and calculated as the average intake of nutrients across diet pairs. The regulated intake point can then be mapped onto the nutritional landscape (white cross, Figure 1C) to determine whether individuals are regulating their intake of nutrients to optimise certain life-history traits. If the regulated intake point coincides with the nutritional optima for a given life-history trait is taken as evidence for optimal nutrient regulation (Simpson and Raubenheimer 2012).

It has been argued that the above framework can also provide insight into the existence and the potential regulation of trade-offs between different life-history traits. That is, when the optimal expression of two life-history traits measured on the same individuals occur in different regions of the nutritional landscape, a nutrient-space trade-off will exist because both traits cannot be optimized at the same intake of nutrients (Lee et al. 2008a; Maklakov et al. 2008; Cotter et al. 2011; Jensen et al. 2015; Bunning et al. 2015; Bunning et al. 2016). It is important to note, however, that two life-history traits being optimized in the same region of the nutritional landscape does not preclude a trade-off existing due to other physiological constraints than nutrition. By estimating and comparing the regulated intake point to the nutritional optima for two traits, it is not only possible to determine if nutrient regulation is optimal for either trait but also if individuals prioritize one trait over the other through dietary choice (Bunning et al. 2015; Bunning et al. 2016). The problem with these approaches, however, is that they are currently based on the visual inspection of the nutritional landscapes, which has the potential to make any outcomes highly subjective. This is because the non-parametric thin-plate splines used to create nutritional landscapes are obtained from flexible interpolating functions that are subject to sampling error, which can create large uncertainty over the actual location of any nutritional optima for the two traits. Consequently, quantifying the existence and magnitude of tradeoffs, as well as the implications of nutrient regulation under dietary choice, requires formally locating the nutritional optima for each life-history trait and quantifying any

divergence that exists when this error is taken into consideration. A robust analytical approach to achieve this, however, is currently lacking.

The decorated cricket (Gryllodes sigillatus) provides an excellent model to examine the nutritional basis of the trade-off between reproduction and immune function in the sexes. Unlike most insect species, male and female reproductive effort can be easily measured in G. sigillatus. Female reproductive effort can be measured as the number of eggs produced in a given time period (Archer et al. 2012a; b), whereas male reproductive effort can be measured as the time spent calling each night to attract a mate (Hunt et al. 2004; Archer et al. 2012a; b). Producing a call is metabolically costly (Kavanagh 1987), and the number of females attracted increases with amount of time spent calling in male G. sigillatus (Sakaluk 1987), as well as in a range of other cricket species (e.g. Bentsen et al. 2006; Jacot et al. 2008). Diet has sex-specific effects on age-dependent reproductive effort in G. sigillatus (Houslay et al. 2015). Females consuming a poor quality diet produce fewer eggs and invest in egg production later in life compared to those consuming a high quality diet, whereas male calling effort increased with age irrespective of diet quality (Houslay et al. 2015). Immune function is sexually dimorphic in G. sigillatus, with females having higher phenyloxidase activity and a greater encapsulation ability than males (Gershman et al. 2010a; Galicia et al. 2014). The reverse pattern, however, appears true for lytic activity (Galicia et al. 2014; but see Gershman et al. 2010a). Although the effect of nutrient intake on immune function has not been thoroughly investigated in G. sigillatus, diet quality (the relative percentage of rabbit food and bran) does not appear to alter phenyloxidase or lytic activity in the sexes (Galicia et al. 2014). We currently do not know, however, if immune function is traded against calling effort in males or egg production in females, or what role (if any) nutrition plays in mediating this trade-off.

In this study, we start by providing an analytical approach to formally document the existence and quantify the strength of life-history trade-offs when using the geometric framework for nutrition. Following convention, we view a life-history trade-off as a negative covariance between the two traits (Stearns 1992). However, because we are focusing on how this covariance is influenced by the intake of specific nutrients, we use the term nutrient-space based trade-offs. We then empirically test the utility of this approach by conducting two experiments to determine the effect of protein (P) and carbohydrate (C) intake on the nutrient-space based trade-off between reproduction and aspects of immune

function in male and female G. sigillatus. In our first experiment, we restrict individual male and female crickets to one of 24 holidic diets differing in P:C ratio and total nutritional content. This created a nutritional landscape with six nutritional rails along which male and female crickets could vary their intake of P and C by eating more or less of a given diet (Table S1, Figure S1). We measured the intake of nutrients during sexual maturation and examined how this influenced reproductive effort (calling effort in males and egg production in females) and several aspects of immune function (inactive and activated phenyloxidase activity and encapsulation ability) in the sexes and the extent to which these traits are subject to a nutrient-space based trade-off. In our second experiment, we examined how the sexes regulate their intake of P and C when given dietary choice. Males and females were given the choice between diets that differed in both the P:C ratio and total nutritional content in four diet pairings (Table S1, Figure S1). The total intake of P and C was again measured for crickets in each diet pairing during sexual maturation and the regulated intake point calculated for each sex and mapped onto their nutritional landscapes for reproduction and measures of immune function (from Experiment 1) to determine whether nutrient regulation is optimal for these life-history traits.

Materials and Methods

Analytical Approach for Quantifying Nutrient-space Based Trade-Offs

We propose that a nutrient-space based life-history trade-off will occur whenever the optimal expression of two life-history traits measured on the same individuals occur in different regions of the nutritional landscape and that this will result in a negative covariance between the two life-history traits being examined. This does not mean, however, that a trade-off due to other physiological constraints than nutrition cannot exist when two life-history traits are optimized in the same region of the nutritional landscape. We argue that three steps are essential to provide a robust analytical approach for quantifying the strength of such trade-offs when using the geometric framework for nutrition. First, the linear and nonlinear effects of nutrient intake on life-history traits need to be estimated in a standardized way. While response surface methodologies offer a simple way to estimate these effects, any resulting parameters will only be comparable across different life-history traits, the sexes, or different species, if nutrient intake and life-history

traits are provided in the same scale. This is because nutrient intake often differs markedly across the sexes and species, and life-history traits are frequently measured on different scales (e.g. days, growth rate and size). While many different approaches exist to standardize biological data, we advocate standardizing nutrient intake and life-history traits to a z-score (z) by subtracting the population mean (μ) from each data point (x_i) and dividing by the standard deviation (σ) of the population ($z = x_i - \mu/\sigma$). Z-scores are therefore provided in units of standard deviations above (positive scores) and below (negative scores) the population mean and have the useful property of altering the scale but not the underlying distribution of the traits being standardized.

Second, when nutritional optima are formally detected for different life-history traits, it is necessary to locate the position of the global maximum for each trait in nutrient space and also to estimate the 95% confidence region (CR) for this maximum. Locating the position of the global maximum is essential for determining the exact intake of nutrients that maximises the expression of a life-history trait. As both the intake of nutrients and lifehistory traits are measured with error, the 95% CR is needed to determine how this uncertainty influences the position of the global maximum. Furthermore, it allows a direct test of whether individuals regulate their intake of nutrients optimally to maximize the trait under dietary choice: the regulated intake of nutrients can be considered optimal if this point resides within the 95% CR for the global maximum. Second order (quadratic) parametric models are typically used to locate the global maximum on a response surface and to estimate the 95% CR of this point (Box and Draper 1987; Peterson et al. 2002). This approach assumes, however, that the data are normally distributed and that the global maximum is best located by a second-order quadratic approximation (Peterson et al. 2002). These assumptions are often not tenable for many nutritional and life-history data sets, but can be overcome by using nonparametric bootstrap methods that are not reliant on a normal distribution and incorporate a flexible regression spline model. We develop a new R package ("OptimaRegion", del Castillo et al. 2016) to perform this analysis with nutritional data (see below).

Finally, the nutritional landscapes for different life-history traits must be formally compared and the magnitude of any differences accurately quantified. A sequential model-building approach (Draper and John 1988) offers a well-established protocol for comparing the linear, quadratic and correlational regression coefficients for different response surfaces

(Draper and John 1988), and this approach has already been used extensively to formally compare nutritional landscapes for different life-history traits within (South et al. 2011; Bunning et al. 2015; House et al. 2016; Rapkin et al. 2016) and across (Rapkin et al. 2016; Bunning et al. 2016) the sexes. A limitation of this approach, however, is that only the sign and magnitude of the regression coefficients are compared. Thus, it is possible that the two life-history traits being compared show different linear and/or nonlinear regression coefficients, but that the global maxima actually occupy the same region in nutrient space. The simplest way to formally demonstrate that the global maxima for two life-history traits occupy different regions in nutrient space is to visually compare the 95% CRs for the global maxima. If the 95% CRs are non-overlapping, this provides clear evidence that the global maxima are located in different regions. It is important to note, however, that the reverse scenario is not always true: overlapping 95% CRs does not necessarily mean that there is no difference in the location of the two global maxima. In such instances, it is particularly important to quantify the exact magnitude of any divergence in the location of the global maxima and we propose two additional measures based on geometric principles to characterise this in simple metric form. First, the divergence between the global maxima in nutrient space can be measured as the angle (θ) between the linear nutritional vectors as:

$$\theta = \cos^{-1}\left(\frac{a \cdot b}{\|a\| \|b\|}\right)$$
 Equation (1)

where a is the linear effects of nutrient intake on the first life-history trait being compared, b is the linear effects of these nutrients for the second life-history trait, $||a|| = \sqrt{a \cdot a}$ and $||b|| = \sqrt{b \cdot b}$. Larger values of θ indicate a greater separation of the optima in nutrient space and therefore a larger trade-off between life-history traits (Figure 2A & B), whereas as θ approaches 0°, the optima become more aligned in nutrient space, indicative of a weaker trade-off between life-history traits. We have already applied this approach to nutritional data (Bunning et al. 2015, 2016; Rapkin et al. 2016). Second, the divergence between the global maxima in two-dimensional nutrient space can be measured as the Euclidean distance (d) between the global maxima for each nutritional landscape as:

$$d = \sqrt{(x_2 - x_1)^2 + (y_2 - y_1)^2}$$
 Equation (2)

where x_1,y_1 and x_2,y_2 are the two nutrient coordinates for the global maxima of the first and second life-history traits being compared, respectively. When the nutritional optima for the two life-history traits are located on similar iso-caloric lines, measures of θ and d will be closely related: a larger θ will be associated with a longer d (Figure 2A-C). However, when the nutritional optima are on different iso-caloric lines, θ may under-estimate the true degree of divergence between optima and d will provide a better metric of this difference (Figure 2D). We provide analytical solutions in Appendix B showing that an increases in θ and d results in a stronger negative covariance between the two life-history traits being examined.

To provide measures of θ and d that are comparable across studies, we propose that these parameters be expressed as a percentage of their maximum value. As θ measures the divergence between linear nutritional vectors, the maximum separation is always 180°. In the case of d, the maximum value will depend on the range of nutrient rails included in the geometric design of diets and how much individuals feed along these rails. Thus, the maximum d will vary between experiments and we propose that the highest intake of nutrients on the two most extreme nutritional rails be used in Equation (2) to calculate the maximum d.

In summary, we propose that nutrient-space based trade-offs occur when the global maxima for two life-history traits measured on the same individuals occur in different regions in nutrient space so that both traits cannot be maximised at a single intake of nutrients. We provide an analytical approach that provides an easy way to formally document the existence and quantify the strength of such nutrient-space based trade-offs when using the geometric framework. We show that two life-history traits will exhibit a large nutrient-space based trade-off when the 95% CRs for the global maxima are not overlapping in nutrient space, there is a large θ between the linear nutritional vectors for the two traits, and/or a large \mathbf{d} between the global maximum for each trait. This framework enables the strength of nutrient-space based trade-offs to be estimated in a standardized way that facilitates direct comparison between different life-history traits when using the geometric framework approach. Furthermore, visually comparing the regulated intake point to the 95% CRs for the global maxima for each life-history trait provides a useful way to

formally demonstrate whether nutrient regulation is optimal for either trait and therefore if individuals are able to prioritize one trait over the other through dietary choice.

Experimental Animals

G. sigillatus used in our experiments were taken from our mass colonies, which are housed in twelve transparent 15L plastic containers in an environmental chamber (Percival I-66VL) maintained at 32 ± 1°C on a 14h:10h light/dark cycle. The crickets in our mass culture are the descendants of approximately 500 adults collected in Las Cruces, New Mexico in 2001, and used to initiate a laboratory culture maintained at a population size of approximately 5000 crickets and allowed to breed panmictically. Crickets were provided with commercial cat food (Go-Cat Senior®, Purina, St Louis, MO, USA) and rat food (SDS Diets, Essex, UK) pellets. Water was provided ad libitum in 60ml glass test tubes plugged with cotton wool, and there was an abundance of egg cartons to provide shelter. As soon as adults were detected, moistened cotton wool was provided in a petri-dish (10cm diameter) as an oviposition substrate. Each generation, crickets were randomly mixed between containers and were maintained at a density of approximately 300 crickets per container.

Experimental animals were collected as newly hatched nymphs from the oviposition pads, housed individually in a plastic container (5cm x 5cm x 5cm), and provided with a piece of cardboard egg carton for shelter and water in a 2.5ml test tube plugged with cotton wool. Crickets were fed dry cat pellets and their enclosure cleaned once a week. Experimental animals were checked daily for newly eclosed adults and these were then randomly allocated to an experiment and diet treatment (see below).

Artificial Diets and Measuring Dietary Intake

We made 24 artificial, dry and granular foods that varied in protein and carbohydrate content following the procedure outlined in Simpson and Abisgold (1985). Proteins consisted of a 3:1:1 mixture of casein, albumen and peptone with digestible carbohydrates consisting of a 1:1 mixture of sucrose and dextrin. All diets contained Wesson's salts (2.5%), ascorbic acid (0.28%), cholesterol (0.55%), and vitamin mix (0.18%). After the appropriate dry weight of protein and carbohydrate had been added to the mixture, the remainder of the mixture was made up to the appropriate dilution with crystalline cellulose. The diets

used in each experiment are presented in Table S1 and Figure S1 shows their distribution in nutrient space.

Each experimental cricket was housed in an individual transparent plastic container (20cm x 10cm x 10cm) and given either one (Experiment 1) or two (Experiment 2) dishes of food of measured dry weight on their first day of adulthood. Food and water were provided in feeding platforms created by gluing the upturned plastic lid of a vial (1.6cm diameter, 1.6 cm deep) in the centre of a plastic petri dish (5.5cm diameter), and changed every 2 days for a total of 16 days. The materials and design of the feeding platforms ensured that experimental animals could not consume anything other than the artificial diet(s) and water, and that food could be collected (in the petri dish) if spilled during feeding. Food was kept in a drying oven at 30°C for 72 hours to remove moisture prior to weighing. Prior to weighing, any faeces were removed from the feeding platform using a pair of fine forceps. Diet consumption was calculated as the difference in dry weight before and after feeding and this was converted to a weight of P and C ingested by multiplying by the proportion of that nutrient in the diet following the protocol outlined in South et al. (2011).

Experiment 1: No Choice of Diet on Six Nutritional Rails

Experimental Design

On the day of eclosion to adulthood (day 0), 15 males and 15 females were randomly allocated to each of the 24 artificial diets (n = 720). Each individual was weighed at eclosion using an Ohaus electronic balance (Explorer* Pro model EP214C) and their pronotum width measured under a dissection microscope (Leica MZ6) fitted with an eyepiece graticule. There was no significant difference in the body size (male: $F_{23,336}$ = 1.02, P = 0.44; female: $F_{23,336}$ = 0.54, P = 0.96) or weight (male: $F_{23,336}$ = 0.89, P = 0.61; female: $F_{23,336}$ = 1.02, P = 0.44) of crickets across diets, thereby confirming our random allocation. On the night of day 7 post-eclosion, each experimental cricket had its diet removed and a virgin cricket of the opposite sex taken at random from the stock population was added to the container to allow mating overnight. On day 8, the mating partners were removed and the experimental individuals provided with their specific diets as normal. We measured reproductive effort in the sexes on day 8 and 9 post-eclosion and aspects of immune function on the same individuals between days 14 to 16 post-eclosion (see below).

Measuring Reproductive Effort

We measured female reproductive effort as the number of eggs produced by a female on days 8 and 9. Each female was provided with a small petri dish (5.5cm diameter) full of moist sand for oviposition. Females had access to this oviposition substrate continuously for this two day period, after which it was removed and replaced with a fresh petri dish every night until the end of the experiment (day 16). This was done to ensure that both sexes had the same potential for reproductive effort between days 8 and 9 and until the end of the experiment (see below). To count eggs, the content of each petri dish was emptied into a round container of water (10cm diameter, 12cm height), swirled in a circular fashion for 20 seconds, and eggs were counted as they moved to the surface of the sand.

Male reproductive effort was measured as the amount of time a male spent calling to attract a mate each night, as this provides a good measure of male mating success (Bentsen et al. 2006). We measured the time each male spent calling on the nights of days 8 and 9 between 18:00 to 09:00 using a custom-built electronic monitoring device (Hunt et al. 2004). Full details of this device are provided in Appendix C.

Measuring Aspects of Immune Function

One enzyme cascade that is particularly important in the insect immune system is the prophenoloxidase cascade (González-Santoyo and Córdoba-Aguilar 2012). Phenoloxidase is a copper-containing enzyme that catalyzes the oxygenation of mono-phenols to *o*-diphenols and the oxidation of *o*-diphenols to *o*-quinones (González-Santoyo and Córdoba-Aguilar 2012). These are the key steps in the synthesis of melanin, a pigment found in the insect cuticle which is also used to encapsulate foreign bodies in the haemolymph (Götz 1986). Both endogenous and exogenous signals are known to trigger the activation of phenoloxidase in insects and this activation occurs rapidly (i.e. minutes to hours) (e.g. Korner and Schmid-Hempel 2004), providing protection against a wide range of pathogens, including nucleopolyhedroviruses (NPVs), fungi, nematodes and parasitoids (e.g. Ourth and Renis 1993; Hagen et al. 1994; Bidochka and Hajek 1998).

Here, we focus our examination of the immune function on the phenoloxidase cascade in *G. sigillatus*. We first measure the amounts of phenoloxidase circulating in the haemolymph before and after the insertion of a foreign body: we refer to these as inactive and activated phenoloxidase, respectively. We then measure how well crickets encapsulate

this foreign body as it is engulfed by hemocytes through melanization. Thus, we examine phenoloxidase from the start to the end of the cascade (Tsakas and Marmaras 2010). It is important to note, however, that our estimates of phenoloxidase activity are "potential" responses because they measure *in vitro* the amount of the enzyme present, providing information about the potential of an individual to mount an immune response. In contrast, our estimate of encapsulation ability measures the response of an individual to a novel immune challenge and thus represents a "realized" immune response. We measured these aspects of the immune function of male and female crickets following the protocol outlined below.

Encapsulation ability

At 14 days of age, crickets were cold-anesthetized at 6°C in a refrigerator for 10 minutes. During this period, an implant of nylon monofilament fishing line (length: 2mm, diameter: 0.3mm) with a surface abraded with sandpaper and a hypodermic needle from a 30.5 gauge syringe were sterilized in 70% ethanol. A small hole was made ventrally between the fifth and sixth abdominal segments of the cricket using the needle, and the implant was inserted into the wound with dissection forceps until it was completely contained within the abdominal cavity of the cricket. After implantation, crickets were returned to their individual containers and provided with fresh diet and water. Previous work using this approach has shown that the greatest variation in melanisation occurs 2 days after implantation (Gershman et al. 2010a). Therefore, 2 days after each cricket was implanted, it was placed in a 3ml microcentrifuge tube and frozen at -20°C. Implants were dissected from frozen crickets and any clumps of tissue removed with paper towel and each implant was photographed and a darkness score calculated following the protocol outlined in Appendix C.

Inactive and activated phenoloxidase activity

During implantation of the nylon monofilament, a 3μ l sample of haemolymph was collected with a glass pipette from the wound and mixed with 40μ l of 1 X Phosphate Buffered Saline solution (PBS) in a 1.5ml microcentrifuge tube. This was used to measure inactive phenoloxidase activity. Two days later, and just before each cricket was frozen, a further 3μ l of haemolymph was extracted and mixed with 40μ l of 1 X PBS in a 1.5ml microcentrifuge

tube. This was used to measure activated phenoloxidase activity. Haemolymph samples were frozen and stored in a -80°C freezer to induce cell lysis and to prevent enzymatic reactions from proceeding. phenoloxidase activity of our haemolymph samples were measured following the protocols outlined in Appendix C.

Experiment 2: Measuring Nutrient Intake Under Dietary Choice

A total of 20 crickets of each sex were assigned at random to one of four diet pairs (total n=160) on their day of eclosion to adulthood. The diets used in these pairs varied in both the P:C ratio and total nutrition (P:C ratio (total nutrition %)): Pair 1: Diet 2 (5:1 (36%)) versus Diet 22 (1:8 (36%)), Pair 2: Diet 2 (5:1 (36%)) versus Diet 24 (1:8 (84%)), Pair 3: Diet 4 (5:1 (84%)) versus Diet 22 (1:8 (36%)), and Pair 4: Diet 4 (5:1 (84%)) versus Diet 24 (1:8 (84%)) (Table S1)). This choice of diet pairs provides a wide coverage in nutrient space (Figure S1). Consumption of both diets was measured every two days for a total of 16 days post-eclosion under similar overall conditions as in Experiment 1, with a random mate being assigned to each experimental cricket overnight on day 7.

Statistical Analyses

Characterizing the linear and nonlinear effects of nutrient intake

We used a multivariate response-surface approach to estimate the linear and nonlinear effects of P and C intake on our response variables (i.e. reproductive effort, encapsulation ability, inactive phenoloxidase activity and activated phenoloxidase activity)(South et al. 2011). Prior to analyses, we standardized nutrient intake and life-history data to a *z*-score (i.e. a mean of zero and standard deviation of one) to ensure that any differences in nutritional gradients were not driven exclusively by scale (South et al. 2011). Non-parametric thin-plate splines (TPS) were used to visualize the nutritional landscapes for each life-history trait that was significantly influenced by nutrient intake. Thin-plate splines were constructed using the "Tps" function in the "fields" package (Nychka et al. 2015) of R (R Core Team, version 2.15.1, Vienna, Austria, www.r-project.org). To aid interpretation, all TPS were constructed using unstandardized data. For each nutritional landscape, we used the smoothness λ value that minimized the generalized cross-validation score (Green and Silverman 1994).

Estimating the location of each nutritional optimum and its 95% CR

To estimate the location of the nutritional optima and their 95% CRs, we develop a novel nonparametric bootstrapping method that does not make any distributional assumptions and uses a flexible regression spline model. This approach is provided by function OptRegionTps in the R package "OptimaRegion" (del Castillo et al. 2016). In brief, this function fits a two-dimensional thin-plate spline model to the experimental data using a penalized roughness approach and the "Tps" function in the "fields" package, where the user is able to define the smoothness parameter λ (for example, obtained by crossvalidation and the Tps function on the experimental data). This function yields the vector of predictions \hat{y} at all the experimental points using the Kimeldorf-Wahba predictor $\hat{y} = T \; \hat{d} \; + \;$ $\Sigma \hat{c}$ where $\hat{\psi} = (\hat{d}, \hat{c})$ are fitted parameters, T is a matrix of polynomial basis functions (up to cubic degree), and Σ is a matrix of radial basis functions computed at all pairs of points x_i (see Nychka 2000 for further details). We compute residuals r_i adjusted for small sample bias (Kauermann et al. 2012). We then applied bootstrapping to these residuals to create bootstrapped realizations $y^*(x) = \hat{y}(x) + r^*$ for each experimental data point (x) in our data set, where $x = (x_1, x_2)$ denotes the P and C intakes on the nutritional landscape. For each simulated set of $y^*(x)$, we fit a TPS(λ) model and found parameter estimates ψ^* . Following Yeh and Singh (1997), we repeated this procedure 1,000 times and computed Tukey's data depth for each generated ψ^* vector, keeping the $100(1-\alpha)$ % deepest (where in our case α = 0.95). This provides an approximate nonparametric bootstrap confidence region for the Tps coefficients ψ . The responses $y^*(x)$ that correspond to the parameter vectors ψ^* inside of their CR were then maximized numerically using the "nloptr" package in R (Johnson 2014; Ypma 2014) with respect to the regressors (x_1, x_2) yielding the bootstrapped response global maxima (x^*) . The nonparametric bootstrapped CR for the location of the global maximum of the fitness function is approximated and displayed as the convex hull of all the bootstrapped peaks (x^*) . We use the centroid (average) of all the maxima located as our point estimate of the global maximum (or nutritional optima) of the nutritional landscape. This constitutes a bagging estimate of the location of the maximum (Hastie et al. 2001).

This procedure for computing the resulting CR is justified by recent work by Woutersen and Ham (2013) who have recently shown that better coverage of bootstrapped CRs of parametric functions (in our case, the vector function $g(x; \psi) = \arg\max_{x \in C} y(x)$ where

 ${\cal C}$ is the experimental region) can be obtained if the bootstrapped values of the function $g(x;\psi)$ are generated from parameters ψ inside their $100(1-\alpha)$ % CR, instead of directly generating an empirical distribution of $g(x;\psi)$ and trimming it to get the desired CR. The rationale behind the Wourtesen and Ham (2013) method is that it is better to sample only from "good" parameters ψ (those inside their CR) and use these for generating the values of $g(x;\psi)$ rather than using both "good" and "bad" generated values of ψ .

Comparing the sign and magnitude of the linear and nonlinear nutritional gradients

We used a sequential model-building approach (Draper and John 1988) to determine whether the linear and nonlinear (quadratic and correlational) effects of nutrient intake differed across our life-history traits within and between the sexes. Full details of this analysis, as applied to nutritional data, are provided in Appendix D and linear equations are provided in South et al. (2011).

Calculating the angle and 95% CIs between linear nutritional vectors

We used a Bayesian approach implemented in the "MCMCglmm" package of R (Hadfield 2010) to determine the magnitude of θ and the degree of certainty associated with this estimate, measured as the 95% CIs. For each life-history trait being compared, we ran a separate linear model ($R \sim \beta_1 P + \beta_2 C + \varepsilon$) using 400,000 Markov chain iterations with a burnin of 20,000, a thinning interval of 25 and a relatively uninformative prior (v = 1, nu = 0.02), to create a posterior distribution of β for each nutrient. We used these distributions in Equation 1 to generate 15,200 values for θ . The median of these values was used as our point estimate of θ and the 95% CIs were estimated using the "HPDinterval" function. The associated R code for this procedure is available in the supplementary text file.

Calculating the Euclidean distance and 95% confidence intervals between global maxima

To determine the mean and median Euclidean distance between the locations of the maxima of two response surfaces, we developed a custom program "CRcompare.R" in the R package "OptimaRegion" (del Castillo et al. 2016). The program starts by calling the function "OptRegionTps.R" from the "OptimaRegion package" (del Castillo et al. 2016) twice, once for each of the two life-history traits being compared, to compute a CR on the maxima of each response surface. These CRs are a set of points obtained by repeatedly bootstrapping

the residuals of the original TPS model, creating sample response data to which new TPS models are fitted and then optimized to obtain the location of their maxima. Our program then computes all possible pairwise Euclidean distances between the response maxima in each CR. Finally, it bootstraps the mean and median of these distances using R's package "boot" (Canty and Ripley 2016) to obtain 95% bias-corrected and accelerated (BCA, see Efron and Tibshirani 1998) bootstrapped confidence intervals on the mean and median distance.

Testing for dietary choice and the non-random intake of nutrients

To determine whether male and female crickets preferentially consumed one of the diets over the other in each diet pair contained in Experiment 2, we compared the absolute consumption of each diet using a paired t-test. However, this approach does not account for the fact that our choice diets have different concentrations of P and C meaning that crickets may actually eat more of a less concentrated diet (i.e. compensatory feeding) to increase their intake of P and/or C. We therefore investigated the non-random intake of nutrients in the sexes in two ways. First, we calculated the total intake of P and C for each diet pair and subtracted the expected intake of these nutrients if crickets fed at random. This difference was compared to a mean of zero (i.e. expected if crickets were feeding at random on diets) using a one-sample t-test. A value greater than zero, therefore, means that a cricket has consumed significantly more P or C than expected, a value less than zero means that a cricket has consumed significantly less than expected, whereas a value that does not differ significantly from zero means that crickets have consumed nutrients equally from both diets. Second, we used a MANOVA to compare the total intake of P and C across the sexes and diet pairs; sex, diet pair and their interaction were included as fixed effects and P and C intake as dependent variables. Univariate ANOVAs were used to determine which nutrients contribute to the overall multivariate effect. As there are four diet pairs, Tukey's HSD contrasts were used to determine how the intake of P and C differed across diet pairs for each sex.

Estimating and comparing the regulated intake point between the sexes

We estimated the regulated intake point in each sex, defined as the point in nutrient space that individuals actively defend when given dietary choice, as the mean intake of P and C

across diet pairs (Simpson and Raubenheimer 2012). We used an ANCOVA including sex as a fixed effect, P intake as a covariate, the interaction between sex and P intake as a fixed effect, and C intake as the dependent variable to determine if the regulated intake point differed significantly across the sexes. Significance of the sex by P intake interaction term demonstrates that the sexes have different regulated intake points.

Determining if nutrient regulation is optimal for trait expression in the sexes

To determine whether males and females optimally regulate their intake of nutrients to maximise trait expression, we mapped the RIP for each sex onto the nutritional landscape containing the 95% CR of the peak (global maximum) for each trait (see Figure 3). We consider nutrient regulation to be optimal for a given trait if the regulated intake point overlaps the 95% CR of the global maximum on the nutritional landscape.

Results

Experiment 1: No Choice of Diet on Six Nutritional Rails

There was a clear significant linear effect of the intake of both nutrients on male calling effort, with the amount of calling increasing with the intake of C but decreasing with the intake of P (Table 1, Figure 3A). There was also a significant negative quadratic effect of C intake on calling effort, and inspection of the nutritional landscape (Figure 3A) reveals a peak in calling effort at a high intake of C and low intake of P centred around a ratio of 1_P: $7.08_{\rm C}$ (global maximum: P = 17.87 mg, C = 126.57 mg, Figure 3A). A significant negative correlational gradient for calling effort (Table 1) provides further evidence that calling effort increases with C intake and decreases with P intake. The encapsulation ability of males increased with the P consumption but was independent of C (Table 1, Figure 3B). There was also a significant negative quadratic effect of P intake on encapsulation ability (Table 1) and inspection of the nutritional landscape (Figure 3B) reveals a peak in encapsulation ability at a high intake of P and low intake of C centred around a ratio of 5.14_P:1_C (global maximum: P = 104.24 mg, C = 20.29 mg, Figure 3B). The significant negative correlational gradient further demonstrates that encapsulation ability is maximized on a high intake of P and low intake of C (Table 1). In contrast to calling effort and encapsulation ability, the intake of P and C did not significantly influence inactive and activated phenoloxidase activity (Table 1).

Formal statistical comparison of the traits that responded to P and C intake, using a sequential model building approach showed significant differences in the linear, quadratic and correlational effects of nutrient intake on male calling effort and encapsulation ability (Table 2). The difference in linear effects was due to encapsulation ability increasing with P intake, but calling effort decreasing with the intake of this nutrient, and also because calling effort increased with C intake, but encapsulation ability did not (Table 2). The difference in quadratic effects reflects that there was a peak in encapsulation ability, but not calling effort, with P intake, and there was a peak in calling effort, but not encapsulation ability, with C intake (Table 2). Finally, the difference in the correlational effects exists because the effect of the negative covariance between P and C intake is stronger on encapsulation ability than on calling effort (Table 2). This pattern of nutritional effects on calling effort and encapsulation ability results in a significant negative correlation between these traits across diets in our geometric design (r = -0.104, 95% CI = -0.154, -0.055, n = 360, P = 0.048) and leads to nutritional optima that are located in different regions in nutrient space (Figure 3A & B) providing evidence of a trade-off between calling effort and encapsulation ability in males. Further evidence of a trade-off between these traits in males is shown, using our proposed methodology, by the large angle between the linear nutritional vectors (θ = 107.20°, 95% CI: 93.26°, 120.53°) and the large Euclidean distance between the global maxima for calling effort and encapsulation ability (d =145.05 mg, 95% CI: 143.60 mg, 146.30 mg), which represents 78.41% and 59.56% of the maximum differences, respectively (maximal possible θ = 180°, maximal possible d = 185.00). Furthermore, comparison of Figures 4A & B shows that there is no visible overlap in the 95% CRs for optimal calling effort and encapsulation ability. Collectively, this provides clear evidence of a trade-off between calling effort and encapsulation ability in males.

In females, reproductive effort increased linearly with the intake of P and C, with egg production being equally responsive to the intake of both nutrients (Table 1, Figure 3C). There were also significant negative quadratic effects of P and C intake on egg production (Table 1) and inspection of the nutritional landscape (Figure 3C) shows a peak in egg production at a high intake of P and C centred around a ratio of $1_P:1.17_C$ (global maximum: P = 126.09 mg, C= 148.09 mg, Figure 3C). The significant positive correlational gradient provides further evidence that egg production is maximised on a high intake of both P and C (Table 1). Female encapsulation ability also increased linearly with the intake of both

nutrients, although this trait was slightly more responsive to the intake of P than C (Table 1). There were also significant negative quadratic effects of P and C intake on encapsulation ability in females (Table 1), and inspection of the nutritional landscape (Figure 3D) shows a peak in encapsulation activity at a high intake of P and C centred around a ratio of $1.04_P:1_C$ (global maximum: P = 129.66 mg, C = 124.70 mg, Figure 3D). There was, however, no significant correlational effect of the two nutrients on female encapsulation ability (Table 1). As for males, the intake of P and C did not significantly influence inactive or activated phenoloxidase activity (Table 1).

Formal statistical comparison, of female traits that responded to P and C intake, showed a significant difference in the linear effects of nutrient intake on female egg production and encapsulation ability, but no difference in the quadratic or correlational effects (Table 2). The difference in linear effects was due to egg production being more responsive to the intake of both nutrients than encapsulation ability (Table 2). This pattern of nutritional effects on egg production and encapsulation ability in females leads to nutritional optima that are located in similar regions of nutrient space (Figure 3C & D), and a significant positive correlation between these traits across diets (r = 0.260, 95% CI = 0.156, 0.361, n = 360, P = 0.0001). Consequently, using our proposed methodology, we found a small angle between the linear nutritional vectors (θ = 16.71°, 95% CI: 0.00°, 34.64°) and a short Euclidean distance between the global maxima for calling effort and encapsulation ability (d = 33.83 mg, 95% CI: 29.90 mg, 37.29 mg), which represents 9.28% and 13.64% of the maximum differences, respectively (maximal possible θ = 180°, maximal possible d = 248.02). Furthermore, the 95% CRs for egg production and encapsulation ability are completely overlapping (Figure 4C & D). Together, these results suggest that egg production and encapsulation ability in females do not trade-off.

Formal statistical comparison using a sequential model building approach also showed significant differences in the linear, quadratic and correlational effects of nutrient intake on reproductive effort and encapsulation ability between the sexes (Table 2). For reproductive effort, the sex difference in the linear effects of nutrient intake is driven exclusively by P intake, having a negative effect on calling effort but a positive effect on egg production (Table 2). The sex difference in the quadratic effect of nutrients is due to a peak in egg production, but not calling effort, with P intake, and also because the peak in egg production with C intake has a more pronounced curvature than the peak for calling effort

(Table 2). The sex difference in the correlational effects of nutrients is due to egg production increasing, but calling effort decreasing, with the covariance between P and C intake (Table 2). For encapsulation ability, the sex difference in the linear effects of nutrient intake is because C intake increases this trait in females but not in males, and because encapsulation ability is more responsive to C intake in males, than in females (Table 2). The sex difference in the quadratic effects of nutrient intake is because there is a peak in encapsulation ability with C intake in females but not in males and also because the curvature of the peak in encapsulation ability with P intake is more pronounced in females than in males (Table 2). The sex difference in the correlational effects of nutrient intake reflects the decrease in encapsulation ability with the covariance between P and C intake in males, but not in females (Table 2). This divergence in the effects of nutrient intake on reproductive effort and encapsulation ability between the sexes leads to nutritional optima that are located in different regions of nutrient space (Figure 1). This results in a large angle between the linear nutritional vectors for reproductive effort (θ = 55.58°, 95% CI: 41.59°, 69.98) and encapsulation ability (θ = 35.00°, 95% CI: 14.81°, 56.53°) in the sexes, as well as large Euclidean distances between the global maxima for reproductive effort (**d** = 119.17 mg, 95% CI: 118.60, 119.6) and encapsulation ability (**d** = 117.72 mg, 95% CI: 115.50, 119.60) in the sexes (Figure 4).

Experiment 2: Measuring Nutrient Intake under Dietary Choice

MANOVA revealed that sex, diet pair and the interaction between these fixed effects all significantly influenced the intake of nutrients when *G. sigillatus* was given dietary choice (Table 3). For each diet pair, females consumed significantly more diet than males (Figure 5A & B), resulting in a higher intake of both P and C in females than males (Figure 6, Table 3). Both sexes consumed significantly more of the high C diet than the high P diet in each diet pair (Figure 5A & B), which resulted in a significantly higher intake of C and a significantly lower intake of P than expected if individuals fed indiscriminately between diets (Figure 5C & D). Despite this clear preference for the C rich diet, significant differences in P and C intake across diet pairs within both sexes show that the intake of nutrients depended on the choice pair and was not tightly regulated at the same P and C intake across diet pairs in the sexes (Table 3, Figure 6). Indeed, Tukey's HSD pairwise contrasts showed that the order of intake amounts across diet pairs was 1<2<4<3 for P and 3<1<4=2 for C in males, and

1=2<4<3 for P and 3<1<4<2 for C in females (Figure 6). The significant interaction term between sex and diet pair in our MANOVA model reflects this different ordering of diet pairs between the sexes (Table 3, Figure 6).

The regulated intake point was estimated at an intake of 29.51 ± 1.30 mg of P and 59.12 ± 1.96 mg of C in males, and 55.06 ± 2.35 mg of P and 101.12 ± 3.17 mg of C in females, which corresponds to an overall regulated ratio of 1_P:2.00_C for males and 1_P:1.84_C for females (Figure 6). ANCOVA showed that the intake of C differed significantly between the sexes ($F_{1,156}$ = 29.96, P = 0.0001) but was not related to P intake ($F_{1,156}$ = 1.85, P = 0.18), nor was there a significant interaction between sex and P intake ($F_{1,156} = 0.78$, P = 0.38). This non-significant interaction term demonstrates that the regulated intake point does not differ between the sexes (Figure 6). In Figure 4, we map the regulated intake points for the sexes onto the nutritional landscapes containing the 95% CR of the peak (global maximum) to determine if males and females are regulating their intake of nutrients to optimize reproductive effort and/or encapsulation ability. In general, the regulated intake point was more closely aligned with the P:C ratio of the global maximum for reproductive effort and encapsulation ability in females than in males (Figure 4). However, with the exception of female encapsulation ability (Figure 3D), the regulated intake point for all other traits in both sexes did not overlap with the 95% CR of the global maximum on the nutrient landscape indicating suboptimal nutrient regulation for either of these traits (Figure 4A,B & C). The optimal regulation of nutrients by females to maximize encapsulation ability should be interpreted with a degree of caution, however, due to the large 95% confidence region associated with the peak expression of this trait (Figure 4D).

Discussion

Here, we develop a novel analytical approach to formally identify and quantify the strength of nutrient-space based trade-offs when using the geometric framework for nutrition. We argue that nutrient-space based trade-offs will occur whenever life-history traits measured on the same individuals are maximised in different regions of nutrient space, as demonstrated by non-overlapping 95% confidence regions (CRs) of the global maxima for the two traits. Moreover, we show that the magnitude of this trade-off can be quantified by the angle between the linear nutritional vectors (θ) and the Euclidean distance (d) between

the global maxima for each trait. We then empirically test the utility of our approach by examining the effects of protein (P) and carbohydrate (C) intake on the trade-off between reproduction and aspects of immune function in male and female decorated crickets (*Gryllodes sigillatus*). The intake of P and C had significant but divergent effects on reproduction and encapsulation ability in both sexes, but did not influence inactive or activated phenoloxidase activity. However, the divergence in the nutritional optima for these traits was much larger in males than females as illustrated by the significant negative correlation between these traits in males, the non-overlapping 95% CRs on the global maxima for these traits and the larger estimates of θ and d in males. Collectively, this provides clear evidence that the trade-off between reproduction and encapsulation ability is sex-specific in G. sigillatus and depends critically on the contrasting demands for the intake of P and C needed to maximise these traits in the sexes.

We found that the linear and nonlinear effects of P and C intake on reproduction in G. sigillatus were highly divergent between the sexes. Male calling effort was maximized at high intake of C and low intake of P in a ratio of 1_P:7.08_C, whereas female egg production was maximised at a high intake of both nutrients in a ratio of 1_P :1.17_C. This divergence was confirmed by significant differences in the linear, quadratic and correlational effects of P and C intake on reproductive effort in the sexes, a large angle (55.58°) between the nutritional linear vectors, and a large Euclidean distance (**d** = 119.17mg) between the global maxima for reproductive effort in the sexes. These differences in the optimal nutritional requirements for reproductive effort in G. sigillatus are reflective of the divergent reproductive strategies of the sexes. A major determinant of mating success in male crickets is the amount of time spent producing an advertisement call (e.g. Bentsen et al. 2006; Jacot et al. 2008), which is known to be metabolically costly (e.g. Kavanagh 1987). To fuel this energetic activity, males require a high intake of C to provide an abundant source of energy that can be rapidly utilized after ingestion (Bonduriansky et al. 2008). In contrast, females require a relatively higher intake of P than males, as this macronutrient plays a key role in stimulating oogenesis and regulating vitellogenesis in insects (Wheeler 1996). The sex differences in the nutritional optima for reproduction that we document for G. sigillatus are consistent with other studies on field crickets (Teleogryllus commodus, Maklakov et al. 2008; Gryllus veletis, Harrison et al. 2014) and Drosophila (D. melanogaster, Reddiex et al. 2013; Jensen et al. 2015). It contrasts, however, with a recent study on the ovoviviparous

cockroach *Nauphoeta cinerea*, where both sexes maximised reproductive success at a high intake of C and low intake of P (1_P:8_C; Bunning *et al.*, 2016) most likely due to the unique action of endosymbionts that help recycle stored nitrogen for P synthesis in this species (Bunning et al. 2016).

We also found that the linear and nonlinear effects of P and C intake on encapsulation ability were divergent between the sexes in G. sigillatus. While a high intake of P was important for encapsulation ability in both sexes, this trait was maximized at a relatively higher intake of P to C in males (5.14_P:1_C) than in females (1.04_P:1_C). As shown for reproduction, this divergence was statistically confirmed by significant differences in the linear, quadratic and correlational effects of P and C intake on encapsulation ability in the sexes. The degree of this divergence in nutrient effects, however, was not as large as documented for reproduction, with a smaller angle between the linear nutritional vectors (35.00°) and a shorter Euclidean distance (d = 117.72mg) between the global maximum for encapsulation ability than reproduction across the sexes. While the link between diet and encapsulation ability is well established in a range of insects (e.g. Anagnostou et al. 2010, Kelly 2016), the specific nutrients responsible for this relationship are seldom identified. In the few existing studies that have used well-defined diets of known composition, immune function is reliant on the intake of P (Lee et al. 2006, 2008b; Cotter et al. 2011). These studies are, however, restricted to the larvae of a single species: the cotton leafworm (Spodoptera littoralis). For example, Lee et al. (2006) found that encapsulation ability, antimicrobial activity and PO activity in S. littoralis were all higher on P biased (5_P:1_C and 2_P:1_C) than C biased diets (1_P:2_C and 1_P:5_C). Likewise, Cotter et al. (2011) found that both lysozyme activity and cuticular melanism (a proxy for the encapsulation process) increased with P intake. Our work, therefore, adds much needed support for the relationship between P intake and encapsulation ability in another insect species, as well as providing the first documented example that this relationship differs between the sexes. Currently, we do not know why this sex difference exists but it is possible that the higher intake of P needed to maximise encapsulation ability in males than females reflects the sexual dimorphism in immune function in this species. Males, on average, have a lower encapsulation ability than females in G. sigillatus (Gershman et al. 2010b), and it is possible that they, therefore, require more P to activate this response compared to females.

In contrast to encapsulation ability, P and C intake had little effect on inactive or activated phenoloxidase activity in G. sigillatus. Previous studies using the geometric framework have also found broadly similar results. For example, in S. littoralis, phenoloxidase activity was not influenced by either the quality of P contained in the diet (casein vs zein, Lee et al. 2008b) nor the absolute intake of P (Cotter et al. 2011; but see Lee et al. 2006). In the closely related African armyworm (Spodoptera exempta), however, phenoloxidase activity was shown to increase with P intake (Povey et al. 2009). The general lack of nutrient effects on phenoloxidase activity may reflect the different and varied physiological functions performed by this enzyme. In addition to their role in the immune system, phenoloxidase is also involved in cuticular melanisation after moulting (e.g. Hiruma and Riddiford 1988), which is known to play an important role in key processes such as evaporative water loss (e.g. Rajpurohit et al. 2016) and thermoregulation (e.g. Yin et al. 2016) in insects. Furthermore, activation of the phenoloxidase cascade in the haemocoel of insects also results in the production of quinones and reactive oxygen species that do not discriminate self from non-self, and hence are also known to destroy self-matter (e.g. Saul and Sugumaran 1989). Given the importance of such processes to fitness, phenoloxidase activity may be tightly regulated and insensitive to nutritional effects to help conserve their function. Clearly, more work is needed to empirically validate this idea.

The large divergence that we document in the nutritional optima for calling effort and encapsulation ability, suggests that males are unable to maximise both of these traits on the same diet. In contrast, the smaller divergence between the nutritional landscapes for egg production and encapsulation suggests that females are able to maximise both of these traits on a single diet. Studies using the geometric framework have taken the inability to maximise two life-history traits on a single diet as evidence of a nutrient-space based trade-off (e.g. Lee et al. 2008a; Maklakov et al. 2008; Cotter et al. 2011; Jensen et al. 2015). While we agree with the conclusion that life-history trade-offs may exist due to opposing nutritional requirements, these studies have not formally shown that a nutrient-space based trade-off actually exists or attempted to quantify the strength of any such trade-off. Using our novel analytical approach we show that the 95% CRs on the global maxima for reproduction and encapsulation ability overlap in females but not in males. Furthermore, we found significant differences in the linear, quadratic and correlational effects of nutrients on reproduction and encapsulation ability in males, but only a difference in the linear effects

in females. Finally, we found that θ and d were both significantly larger in males than females, as demonstrated by their non-overlapping 95% CRs. Collectively, this provides strong evidence for the presence of a nutrient-space based trade-off between reproduction and encapsulation ability in males, but not in females, a finding that is confirmed by the negative correlation between these traits in males and a positive correlation in females. This result is consistent with sexual selection theory, which predicts that males should invest more in sexual advertisement at the expense of immune function than females (e.g. Rolff 2002; Zuk and Stoehr 2002; Zuk 2009). While our study is the first to use the geometric framework to examine the nutritional basis of sex differences in the trade-off between reproduction and immune function, a number of studies have examined the trade-off between lifespan and reproduction (Maklakov et al. 2008; Harrison et al. 2014; Jensen et al. 2015). In all of these studies, however, the opposite pattern was found, with the nutrient-space based trade-off between lifespan and reproduction being larger in females than in males.

Not surprisingly given the important effects that P and C intake have on reproduction and encapsulation ability, we found that both sexes actively regulate their intake of these nutrients when given dietary choice. Both sexes, however, were shown to regulate their intake of nutrients to the same nutrient ratio (males: 1_P:2.00_C and females 1_P:1.84_C). Despite this regulation, mapping of the regulated intake points for each sex onto the nutritional landscapes for reproduction and encapsulation ability shows this nutrient regulation did not optimise these traits either sex. More specifically, the regulated intake point did not overlap with the 95% CR for the global maximum for reproduction or encapsulation ability, the only exception being encapsulation ability in females that was characterised by a considerably larger 95% CR (Figure 3D). In each instance, the regulated intake point was markedly lower than the intake of nutrients needed to maximise these traits, and the P:C ratio of the regulated intake point also did not align well with the optimal P:C ratios for reproduction and encapsulation ability, especially in males. There are a number of possible reasons to explain these patterns. First, the lower absolute intake of P and C than is optimal may represent physiological constraints on feeding behaviour. It is well established that dietary assimilation, digestion, absorption and utilization can all constrain ingestion in animals (Henson and Hallam 1995), and that the efficiency of these processes is influenced by gut morphology (e.g. Penry and Jumars 1990). It is possible,

therefore, that gut morphology and its effects on these physiological processes prevent individuals from ingesting more nutrients. Second, it is possible that the sexes in G. sigillatus are regulating the relative intake of P to C to maximise other, more heavily prioritised traits. In male G. sigillatus, mating success and cuticular hydrocarbon (CHC) expression are maximised at a ratio of 1_P:1.5_C (Rapkin et al. 2017), and ampulla attachment time (which determines the number of sperm transferred to the female) is maximised at a P:C ratio of 1_P:1.3_C (Rapkin et al. 2016). It is possible, therefore, that males regulate their intake of nutrients to maximise these traits at the expense of calling effort and encapsulation ability. By comparison, lifespan is maximised at a ratio of 1_P:8_C in female G. sigillatus (Hunt, unpublished data), so it is possible that females prioritise this trait over egg production and encapsulation ability when regulating their intake of nutrients. Third, both sexes may be regulating their intake of nutrients to balance the expression of both reproduction and encapsulation ability. In support of this view, the regulated intake points we estimate for males and females is close to midway between the optimal P:C ratio for reproduction and encapsulation ability at 1_P:1.32_C and 1_P:1.06_C, respectively. Finally, it is possible that nutrient regulation under active dietary choice is genetically constrained. If the genes for nutrient regulation are positively genetically correlated across the sexes, but the effects of nutrients on life-history traits are divergent between the sexes, this will generate intralocus sexual conflict (Bonduriansky and Chenoweth 2009) over the optimal intake of nutrients that may prevent the regulated intake point in the sexes from evolving to the optima for reproduction and encapsulation ability. There is currently, however, little support for this process in the single species where it has been thoroughly examined (D. melanogaster, Reddiex et al. 2013), so further work is needed to test this possibility in *G. sigillatus*.

In conclusion, our work provides an analytical approach for studying nutrient-space based life-history trade-offs, as well as statistical tools to do so. Largely due to recent developments in the geometric framework for nutrition, we now have a much better understanding of how the intake of specific nutrients influences life-history traits. We are now in the unique position where the integration of the geometric framework with existing life-history theory is very much needed if we are to further progress in our understanding of how nutrition regulates the trade-off between life-history traits. A particular strength of our analytical approach is that θ and d are measured in standardized units and can be expressed as a percentage of the maximum value that is set by geometric design of the diets used. For

example, the estimates of θ and d were 78.14% and 59.56% of their maximum values in males suggesting that the nutrient-space based trade-off between reproduction and encapsulation ability is actually much stronger than suggested by the phenotypic correlation between these traits (r = -0.104). This standardization facilitates the direct comparison of the strength of nutrient-space based trade-offs across different species and studies using different dietary designs, and thereby offers a flexible path forward for empiricists working on a range of different systems. It has long been argued that it is best to examine life-history trade-offs using experimental manipulation or a quantitative genetic design (e.g. Reznick 1985). While our current study did not adopt either of these designs and therefore provides weaker inference for life-history evolution in G. sigillatus (because the use of animals from mass colonies can bias estimates of correlations by masking line-specific variation in nutrient consumption and trait expression), the analytic approach we outline is also amenable to employing such designs in future studies. For example, nutrient-space based trade-offs can be examined by comparing nutritional landscapes across different levels of immune challenge (e.g. single versus multiple challenges) or by incorporating genetic relatedness (e.g. full-sib genetic design or inbred lines), although this obviously becomes far more logistically demanding.

Acknowledgments

SKS was funded by the National Science Foundation (NSF; IOS-1118160 and IOS-1654028). CMH by a Leverhulme Early Career Fellowship. JH was funded by a Royal Society Fellowship (UF120087) and Equipment Grant (RG090854) and by NERC (NE/G00949X/1). JR was funded by a NERC studentship (awarded to JH). EDC was partially funded by NSF grant CMII 1634878.

Data Archiving

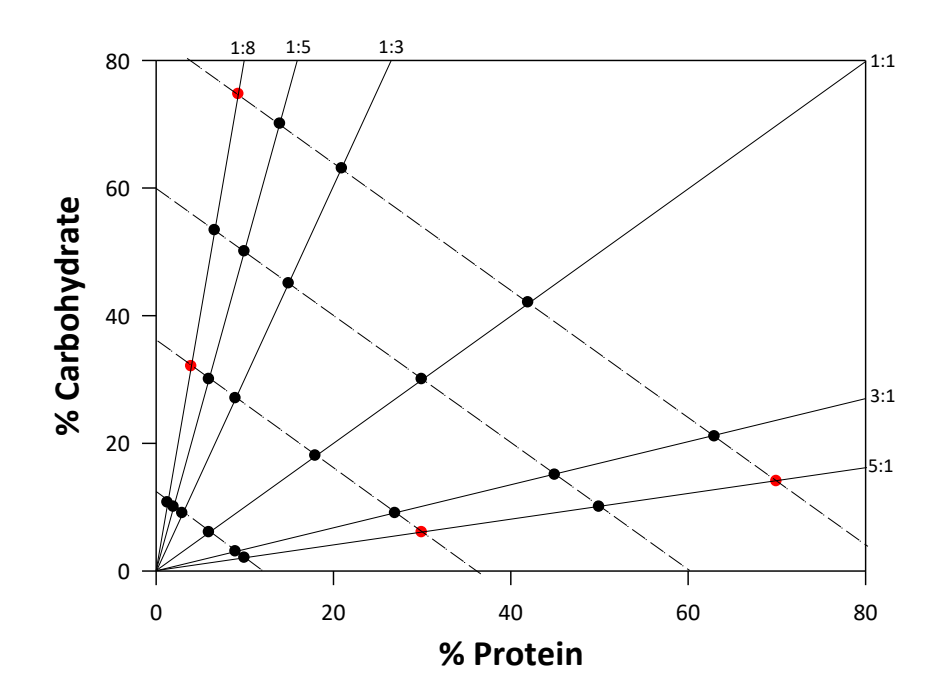
All data are available from the Dryad Digital Repository: DOI: doi:10.5061/dryad.qv437

Appendix A: The composition and distribution in nutrient space of the 24 artificial diets using in our feeding experiments

Table A1. Percentage composition of protein and carbohydrate of the 24 artificial diets used in our feeding experiments. The total nutrients present in each diet are given as the sum of the percentage protein and percentage carbohydrate, with the remaining percentage consisting of indigestible crystalline cellulose. The four diets used in the choice experiment are highlighted with bold text.

	Percen			
Diet	Р	С	P+C	P:C ratio
number				
1	10	2	12	5:1
2	30	6	36	5:1
3	50	10	60	5:1
4	70	14	84	5:1
5	9	3	12	3:1
6	27	9	36	3:1
7	45	15	60	3:1
8	63	21	84	3:1
9	6	6	12	1:1
10	18	18	36	1:1
11	30	30	60	1:1
12	42	42	84	1:1
13	3	9	12	1:3
14	9	27	36	1:3
15	15	45	60	1:3
16	21	63	84	1:3
17	2	10	12	1:5
18	6	30	36	1:5
19	10	50	60	1:5
20	14	70	84	1:5
21	1.33	10.66	12	1:8
22	4	32	36	1:8
23	6.66	53.33	60	1:8
24	9.33	74.66	84	1:8

Figure A1. The distribution of the 24 artificial diets used in our no-choice feeding trial (Experiment 1). The diets are distributed along 6 nutritional rails (solid, black lines), with 4 diets per rail that differ in total nutritional content. The diets that are on different nutrient rails but connected by the iso-caloric lines (dashed, black lines) have equal total nutrition (i.e. P+C). The 4 diets marked with red symbols represent those used in diet pairs in our choice experiment feeding trial (Experiment 2).



Appendix B: Analytical solutions showing that increasing d and θ (i.e. more divergent nutritional optima) reflect a more negative covariance between life-history traits.

Distance between two optima as a function of correlation between responses

In order to show a relation between the correlation amid two traits and the distance and angle between their optima, we assume both trait responses follow a correlated random main effects model with equal curvature. Specifically, suppose we have two traits each modeled as a second order response in two covariates x_1 and x_2 (representing P and C):

$$Y_1 = \beta_0^{(1)} + \beta_1^{(1)} x_1 + \beta_2^{(1)} x_2 + \beta_{12} x_1 x_2 + \beta_{11} x_1^2 + \beta_{22} x_2^2 + \varepsilon_1$$

and

$$Y_2 = \beta_0^{(2)} + \beta_1^{(2)} x_1 + \beta_2^{(2)} x_2 + \beta_{12} x_1 x_2 + \beta_{11} x_1^2 + \beta_{22} x_2^2 + \varepsilon_2$$

where we assume the main effects are random and may be correlated according to a zero mean multivariate normal:

$$\begin{pmatrix} \beta_1^{(1)} \\ \beta_2^{(1)} \\ \beta_1^{(2)} \\ \beta_2^{(2)} \end{pmatrix} \sim N(\mathbf{0}, \mathbf{\Sigma}_{\beta})$$

where

$$\mathbf{\Sigma}_{\beta} = \begin{pmatrix} \mathbf{\Sigma}_{11} & \mathbf{\Sigma}_{12} \\ \mathbf{\Sigma}_{21} & \mathbf{\Sigma}_{22} \end{pmatrix}$$

and the cross-covariances between the main effects are:

$$\Sigma_{12} = \begin{pmatrix} \text{Cov}(\beta_1^{(1)}, \beta_1^{(2)}) & \text{Cov}(\beta_1^{(1)}, \beta_2^{(2)}) \\ \text{Cov}(\beta_2^{(1)}, \beta_1^{(2)}) & \text{Cov}(\beta_2^{(1)}, \beta_2^{(2)}) \end{pmatrix}$$

We assume all variances on the diagonal of Σ_{β} are ones, so all covariances are correlations. We further assume the two responses have equal and non-random curvature, so β_{12} , β_{11} and β_{22} are fixed and common to both responses (the intercepts are also assumed fixed). To simplify the analysis, but without loss of generality, define $\mathbf{b}_i = (\beta_1^{(i)}, \beta_2^{(i)})$ and assume the matrix of quadratic coefficients is:

$$\mathbf{B} = \begin{pmatrix} \beta_{11} & \beta_{12}/2 \\ \beta_{12}/2 & \beta_{22} \end{pmatrix} = \begin{pmatrix} -\frac{1}{2} & 0 \\ 0 & -\frac{1}{2} \end{pmatrix}$$

Since ${\bf B}$ is negative definite, both responses are concave and have a global maximum. The maxima are located at:

$$\mathbf{x}_i^* = -\frac{1}{2}\mathbf{B}^{-1}\mathbf{b}_i = \mathbf{b}_i, \quad i = 1,2.$$

and are therefore two random vectors. The square distance between the two optima is then given by

$$\delta^2 = ||\mathbf{x}_2^* - \mathbf{x}_1^*||^2 = ||\mathbf{b}_2 - \mathbf{b}_1||^2$$

(where $||\cdot||$ denotes the squared Euclidean norm). The expected square distance equals to:

$$E[\delta^2] = E[||\mathbf{x}_2^* - \mathbf{x}_1^*||^2] = ||\mathbf{\mu}_{\beta}||^2 + \operatorname{trace}(\mathbf{\Sigma}_{2-1}) = \operatorname{trace}(\mathbf{\Sigma}_{2-1})$$

where $\mu_{\beta}=E[\mathbf{x}_2^*-\mathbf{x}_1^*)]$ (=0) and $\mathbf{\Sigma}_{2-1}=\mathrm{Var}(\mathbf{x}_2^*-\mathbf{x}_1^*)=\mathrm{Var}(\mathbf{b}_2-\mathbf{b}_1)$. This variance can be shown to be equal

$$\operatorname{Var} \begin{pmatrix} \beta_1^{(2)} - \beta_1^{(1)} \equiv a_1 \\ \beta_2^{(2)} - \beta_2^{(1)} \equiv a_2 \end{pmatrix} = \begin{pmatrix} \operatorname{Var}(a_1) & \operatorname{Cov}(a_1, a_2) \\ \operatorname{Cov}(a_1, a_2) & \operatorname{Var}(a_2) \end{pmatrix}$$

where under our assumption of unit variances we have

$$Var(a_i) = Var(\beta_i^{(1)}) + Var(\beta_i^{(2)}) - 2Cov(\beta_i^{(1)}, \beta_i^{(2)}) = 2(1 - \rho(\beta_i^{(1)}, \beta_i^{(2)}), \quad i = 1, 2$$

(with $\rho(\cdot,\cdot)$ denoting correlation between two random variables) and therefore the expected squared distance between the two optima is:

(1)
$$E[\delta^2] = \operatorname{trace}(\mathbf{\Sigma}_{2-1}) = \sum_i \operatorname{Var}(a_i) = 4 - 2 \left[\rho(\beta_1^{(1)}, \beta_1^{(2)}) + \rho(\beta_2^{(1)}, \beta_2^{(2)}) \right]$$

Assuming $Cov(\varepsilon_1, \varepsilon_2) = 0$ and that the errors are also uncorrelated with any main effect, the covariance between the two responses at covariates $\mathbf{x} = (x_1, x_2)'$ is given by:

$$\begin{array}{lll} \text{Cov}(Y_{1},Y_{2}) & = & E[(\beta_{1}^{(1)}x_{1}+\beta_{2}^{(1)}x_{2})(\beta_{1}^{(2)}x_{1}+\beta_{2}^{(2)}x_{2})] \\ & = & x_{1}^{2}\text{Cov}(\beta_{1}^{(1)},\beta_{1}^{(2)})+x_{1}x_{2}(\text{Cov}(\beta_{1}^{(1)},\beta_{2}^{(2)})+\text{Cov}(\beta_{2}^{(1)},\beta_{1}^{(2)}))+x_{2}^{2}\text{Cov}(\beta_{2}^{(1)},\beta_{2}^{(2)}) \\ & = & x_{1}^{2}\rho(\beta_{1}^{(1)},\beta_{1}^{(2)})+x_{1}x_{2}(\rho(\beta_{1}^{(1)},\beta_{2}^{(2)})+\rho(\beta_{2}^{(1)},\beta_{1}^{(2)}))+x_{2}^{2}\rho(\beta_{2}^{(1)},\beta_{2}^{(2)}) \\ & = & x'\mathbf{\Sigma}_{12}\mathbf{x} \end{array}$$

where the third equality follows because of our assumption of unit variances, so all covariances are correlations. We can now show how there is an inverse relation between $Cov(Y_1, Y_2)$ and the squared expected distance between the optima.

Proposition 1. Under the stated assumptions regarding the two response models Y_1 and Y_2 , $Cov(Y_1, Y_2)$ is a monotonically decreasing function of $E[\delta^2]$ in $(0, \infty)$ for all $(x_1, x_2) \in \mathbb{R}^2$.

Proof. From (1) we have that $\rho(\beta_1^{(1)},\beta_1^{(2)})=\rho(\beta_2^{(1)},\beta_2^{(2)})-E[\delta^2]/2+2$ and $\rho(\beta_2^{(1)},\beta_2^{(2)})=\rho(\beta_1^{(1)},\beta_1^{(2)})-E[\delta^2]/2+2$. Substituting these two expressions into (2) we get

$$Cov(Y_1, Y_2) = x_1^2(\rho(\beta_2^{(1)}, \beta_2^{(2)}) - E[\delta^2]/2 + 2) + x_2^2(\rho(\beta_1^{(1)}, \beta_1^{(2)}) - E[\delta^2]/2 + 2) + x_1x_2(\rho(\beta_1^{(1)}, \beta_2^{(2)}) + \rho(\beta_2^{(1)}, \beta_1^{(2)}))$$

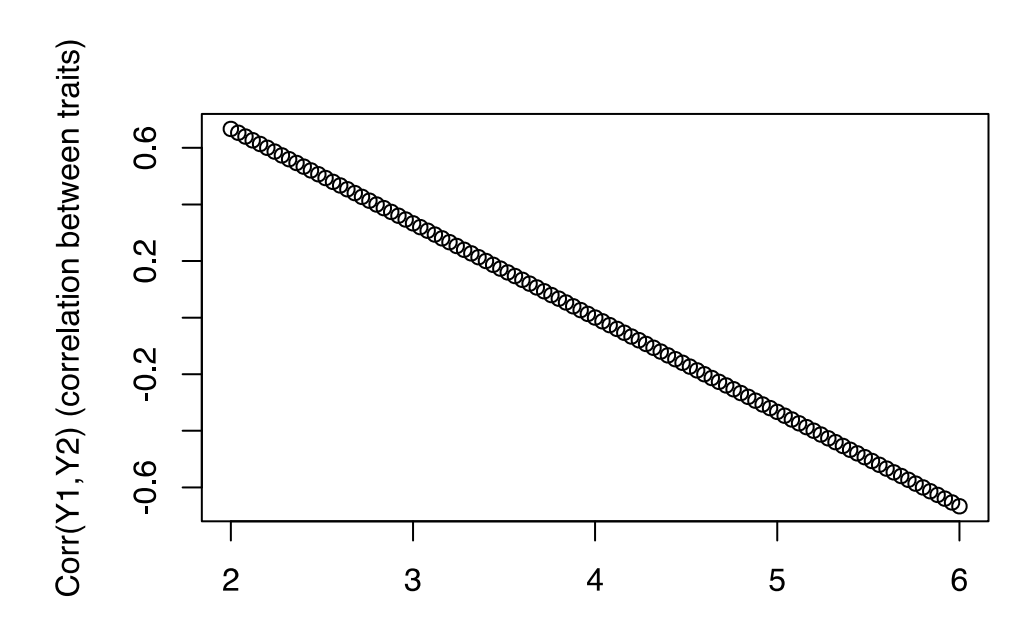
Therefore,

$$\frac{\partial \operatorname{Cov}(Y_1, Y_2)}{\partial E[\delta^2]} = -\frac{x_1^2 + x_2^2}{2} < 0 \quad \forall (x_1, x_2) \in \mathbb{R}^2.$$

and this shows the desired result.

This result implies that increasingly more negative correlated responses have optima that are on average separated by longer distances. The figure below illustrates this inverse relation for the stated assumptions for $x_1 = x_2 = 1$.

Figure B1. Relation between covariation of two traits and the expected squared distance between their optima for the case of two covariates.



E[delta^2] (expected squared distance between optima)

Angle between two optima as a function of correlation between responses

We make the same assumptions regarding the two response models and the covariances of the main effects as in the previous section. The expected cosine of the angle between the two optima θ is given by

$$E[\cos \theta] = E\left[\frac{\mathbf{x}_1^{*'}\mathbf{x}_2^{*}}{||\mathbf{x}_1^{*}|| ||\mathbf{x}_2^{*}||}\right] = E\left[\frac{\mathbf{b}_1'\mathbf{b}_2}{||\mathbf{b}_1|| ||\mathbf{b}_2||}\right]$$

Obtaining an exact expression for this expectation is difficult, given that it is a ratio of random variables. We approximate it simply by

$$E\left[\frac{\mathbf{b_1'b_2}}{||\mathbf{b_1}||\ ||\mathbf{b_2}||}\right] \approx \frac{E[\mathbf{b_1'b_2}]}{E[||\mathbf{b_1}||\ ||\mathbf{b_2}||]} \approx \frac{E[\mathbf{b_1'b_2}]}{E[||\mathbf{b_1}||\ E[||\mathbf{b_2}||]} \approx \frac{E[\mathbf{b_1'b_2}]}{\sqrt{E[||\mathbf{b_1}||^2]}\ \sqrt{E[||\mathbf{b_2}||^2]}}$$

The expected value of the ratio is not the ratio of the expected values, and the expected value of the product is not the product of the expected values. However, this approximation is quite close under our stated assumptions as we show below. First, from Corollary 2.2 in Mathai (1992), who studied distributions of normal bilinear forms, we have that

$$E[\mathbf{b}_1'\mathbf{b}_2] = \operatorname{trace}(\mathbf{\Sigma}_{12})$$

We also have that $E[||\mathbf{b}_i||^2] = \mathrm{Var}(\beta_i^{(1)}) + \mathrm{Var}(\beta_i^{(2)})$ for i=1,2 and these equal 2.0 under our variance assumption. Therefore, we have that $E[||\mathbf{b}_i||] \approx \sqrt{E[||\mathbf{b}_i||^2]} = \sqrt{2}$ and therefore $E[||\mathbf{b}_1||] \ E||\mathbf{b}_2||] \approx 2$. With all this, we have that

(3)
$$E[\cos \theta] = E\left[\frac{\mathbf{b}_{1}'\mathbf{b}_{2}}{||\mathbf{b}_{1}|| \ ||\mathbf{b}_{2}||}\right] \approx \frac{\operatorname{trace}(\mathbf{\Sigma}_{12})}{2}$$
 and
$$E[\theta] \approx \operatorname{acos}\left(\frac{\operatorname{trace}(\mathbf{\Sigma}_{12})}{2}\right)$$

We can show the following relation between the covariance of the responses and the approximate expected angle between the optima.

Proposition 2. Under the stated assumptions regarding the two response models Y_1 and Y_2 , $Cov(Y_1, Y_2)$ is a monotonically decreasing function of the approximated $E[\theta]$ in $(-\pi, \pi)$ for all $(x_1, x_2) \in \mathbb{R}^2$.

Proof. From (3) we have that $\rho(\beta_1^{(1)}, \beta_1^{(2)}) = 2E[\cos \theta] - \rho(\beta_2^{(1)}, \beta_2^{(2)})$ and $\rho(\beta_2^{(1)}, \beta_2^{(2)}) = 2E[\cos \theta] - \rho(\beta_1^{(1)}, \beta_1^{(2)})$. Substituting these two expressions into ([covy1y2]) we get

$$Cov(Y_1, Y_2) = x_1^2 (2E[\cos \theta] - \rho(\beta_2^{(1)}, \beta_2^{(2)})) + x_2^2 (2E[\cos - \rho(\beta_1^{(1)}, \beta_1^{(2)})) + x_1 x_2 (\rho(\beta_1^{(1)}, \beta_2^{(2)}) + \rho(\beta_2^{(1)}, \beta_1^{(2)}))$$

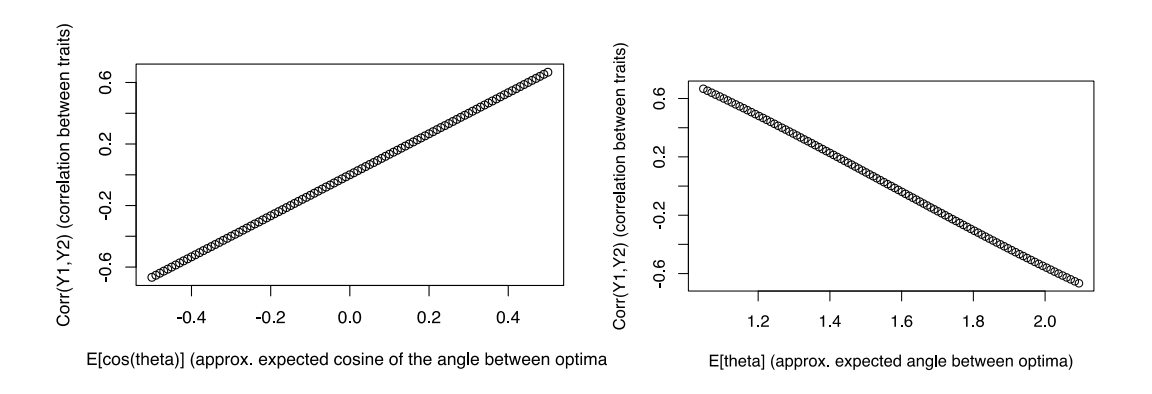
Therefore,

$$\frac{\partial \operatorname{Cov}(Y_1, Y_2)}{\partial E[\cos \theta]} = 2(x_1^2 + x_2^2) > 0 \quad \forall (x_1, x_2) \in \mathbb{R}^2.$$

Since acos(h) is a monotonically decreasing function in (-1,1), then $Cov(Y_1, Y_2)$ is monotonically decreasing in $E[\theta]$ for $\theta \in (-\pi, \pi)$.

The figure below shows the proportional relation between $Cov(Y_1, Y_2)$ and the approximated expected cosine of the angle and the inverse relation between $Cov(Y_1, Y_2)$ and the approximated expected angle for the stated assumptions for $x_1 = x_2 = 1$.

Figure B2. Relation between covariation of two traits and the approximate cosine of the angle between their optima (left) and between covariation of two traits and the expected angle (right) between their optima for the case of two covariates.



Evaluation of the approximation used in (3)

To evaluate the quality of the approximations used to determine the relation between $\operatorname{Cov}(Y_1,Y_2)$ and the expected angle between the optima, $E[\theta]$, we conducted a Monte Carlo simulation of pairs of optima $\mathbf{x}_i^* = \mathbf{b}_i$, for i=1,2 from normally distributed main effects as in the previous section. We then computed both the exact angle spanned by the two optima θ and its cosine, and compared their average values with the approximated expressions developed before. As it can be seen from the table below, the approximation matches the exact angle (and its cosine) for extreme cases when the cross-correlations between the main effects (those in Σ_{12}) are at their extrema of ± 1 . For more moderate correlations, the error in the approximations has a maximum of about 20% for the expected cosine. Given that that qualitatively the approximation matches the behavior (magnitude and sign) of the long-run average cosine, and that quantitatively the errors are small, this approximation suffices to show the main idea behind Proposition 2, namely, that increasingly more negative correlated responses have optima that are on average separated by larger angles. We have also confirmed this general conclusion via simulation.

Table B1. Evaluation of approximation (3) using simulation for different cross-correlations between the main effects. 10,000 multivariate normals were simulated and the average cosine $\overline{cos(\theta)}$ and average angle $\overline{\theta}$ between the corresponding maxima of Y_1 and Y_2 were computed, assuming (as above) that $\boldsymbol{x}_i^* = \boldsymbol{b}_i$, for i = 1,2.

(1) (2)	(1) (2)	(1) (2)	(1) (2)			$E[cos(\theta)]$	Err.
$\rho(\beta_1^{(1)}, \beta_1^{(2)})$	$\rho(\beta_1^{(1)}, \beta_2^{(2)})$	$ \rho(\beta_2^{(1)}, \beta_1^{(2)}) $	$\rho(\beta_2^{(1)}, \beta_2^{(2)})$	$cos(\theta)$	$(\overline{\theta})$	$= trace(\mathbf{\Sigma}_{12})$	(%)
0	0	0	0	0	90	0	0
1	0	0	1	1	0	1	0
-1	0	0	-1	-1	2π	-1	0
0.5	0.25	0.25	0.5	0.414	59	0.5	20
1	0	0	-1	0	90	0	0
0.25	0.25	0.25	0.25	0.204	75	0.25	22
0.5	-0.5	-0.5	0.5	0.461	55	0.5	8
-0.5	0.5	0.5	-0.5	-0.43	123	-0.5	14

Appendix C: Expanded experimental methodologies

Measuring male calling effort

We measured the time each male spent calling on the nights of days 8 and 9 between 18:00 to 09:00 using a custom-built electronic monitoring device (Hunt et al., 2004). Each male was placed in an individual recording chamber (5cm x 5cm x 5cm), with a condenser microphone (c1163, Dick Smith) embedded in the lid, on each night of sampling. Each recording chamber was placed inside a larger foam container (15cm x 15cm x 15cm) to ensure each male was acoustically isolated. Each microphone was connected via acoustic leads to a data acquisition unit (DagBook 120, IO-Tect, Cleveland) and computer (Dell™ OptiPlex™580). The data acquisition unit activates a single microphone at a time, which then relays the sound level to the PC board, where it is compared to background noise. If the received signal is ≥10 dB louder than background noise, this is recorded as a call. The microphone is then deactivated and the next one in the series is activated, with each recording chamber being sampled and recorded 10 times per second, which allowed the number of seconds a male was calling each night between 18:00 to 09:00 to be estimated. During this sampling period, males were not given access to food, but water was provided in a small tube bunged with cotton. To ensure consistency over the length of time both sexes had access to food, we also covered the female's diet during the call sampling period.

Measuring encapsulation ability

Two days after each each cricket was implanted, it was placed in a 3ml microcentrifuge tube and frozen at -20°C. Implants were dissected from frozen crickets and any clumps of tissue removed with paper towel. Each implant was photographed using PixeLink Capture SE software (Version 2.2) three times from three different sides next to a clean implant control using a camera (PixeLink Megapixel Firewire Camera) mounted on a dissecting microscope (Leica MZ6). Each implant and control was outlined using the ImageJ (http://rsbweb.nih.gov/ij/) polygon tool. The darkness of each experimental and control implant (which reveals the extent of encapsulation and melanisation by hemocytes), was measured as the average grayscale value of all the pixels within each image using ImageJ. The darkness score for each individual was calculated as the average grayscale of the three implants' darkness scores, subtracted from the average greyscale of the three control implants' darkness scores. Therefore, darker implants yielded higher darkness scores. A pilot study in which two implants were inserted into opposite sides of each of 20 crickets, and levels of melanisation assessed after 2 days following the above protocol, showed that the repeatability (R) of this method was high (R = 0.93, 95% CI: 0.89, 0.97) (Wolak et al., 2012).

Measuring phenyloxidase (PO) activity

To measure the PO activity of our haemolymph samples, 58mg of 3, 4-Dihydroxyl-L-phenylalanine (L-Dopa) was dissolved in 20 ml of 1 X PBS in a 50 ml conical flask, which was capped with parafilm and immediately covered in aluminium foil due to this solution being photosensitive. The haemolymph samples were defrosted, vortexed and spun down while the L-Dopa was mixing. A total of 5μ l of each haemolymph sample was pipetted into a separate well of a 96 well plate, with the last row of the plate filled with 5μ l of PBS as a

control. Each sample was mixed three times with the pipette before pipetting, and the plate was filled rapidly to minimize evaporation and avoid air bubbles. Using a multichannel pipette, 90μ l of L-Dopa solution was added to each well of the 96 well-plate, with each sample mixed twice with the pipette. The optical density (OD) was then recorded at 490nm using a spectrophotometer (SpectraMax M2) and the programme SoftMax Pro 5.4 (MDS Analytical Technologies). This method estimates the total change in OD over the course of the reaction, with OD readings taken every 10 minutes over a 210 minute period. The average slope of the change in OD over time for the control row was calculated and subtracted from the change in OD slope of a given haemolymph sample to extract the corrected OD slope, with a larger slope indicating more PO activity. Each haemolymph sample was tested twice to calculate an average OD slope for analysis, and all samples were randomized within and across plates before measuring average OD. A pilot study in which we measured inactive and activated PO activity from two independent haemolymph samples for each of 20 crickets using the above protocol, showed high repeatability of this method (Inactive-PO: R = 0.96, 95% CI: 0.93, 0.99, Activated-PO: R = 0.93,95% CI: 0.86, 0.97).

Appendix D: Sequential model-building approach for comparing the linear and nonlinear effects of P and C intake across life-history traits within and between the sexes.

We started the sequential model building approach by first fitting a linear model to the data, including a dummy variable (response type or sex) as a fixed effect, P and C intake as covariates, and our response measures as the dependent variable. From this reduced model, we extracted the residual sums of squares (SS_r). We then ran a second linear model that included all the interactions between the dummy variable and the covariates and again extracted the residual sums of squares for this complete model (SS_c). A partial F-test was then used to statistically compare SS_r and SS_c , where the number of terms added to the complete model and the error degrees of freedom from the complete model are used as the numerator and denominator degrees of freedom, respectively. A significant reduction in SSc compared to SS_r indicates that the complete model significantly increases the amount of variance explained and therefore demonstrates that the nutritional gradients differ significantly across the dummy variable used. This model was repeated by sequentially adding the quadratic terms for nutrient intake (P x P and C x C) and then the correlational term (P x C). In instances where an overall significant difference was detected in the complete model, univariate analyses were used to determine which nutrient (P, C or both) contributed to this effect.

References

- Adamo, S. A., M. Jensen, and M. Younger. 2001. Changes in lifetime immunocompetence in male and female *Gryllus texensis* (formerly G-integer): trade-offs between immunity and reproduction. Animal Behaviour 62: 417–425.
- Anagnostou, C., E. A. LeGrand, and M. Rohlfs. 2010. Friendly food for fitter flies?—Influence of dietary microbial species on food choice and parasitoid resistance in *Drosophila*.

 Oikos 119: 533–541.
- Archer, C. R., S. K. Sakaluk, C. Selman, N. J. Royle, and J. Hunt. 2012a. Oxidative stress and the evolution of sex differences in life Span and ageing in the decorated cricket, *Gryllodes sigillatus*. Evolution 67: 620–634.
- Archer, C. R., F. Zajitschek, S. K. Sakaluk, N. J. Royle, and J. Hunt. 2012b. Sexual selection affects the evolution of lifespan and ageing in the decorated cricket *Gryllodes* sigillatus. Evolution 66: 3088–3100.
- Bateman, A. J. 1948. Intra-sexual selection in *Drosophila*. Heredity 2: 349–368.
- Behmer, S. T. 2009. Insect herbivore nutrient regulation. Annual Review of Entomology 54: 165–187.
- Bentsen, C. L., J. Hunt, M. D. Jennions, and R. Brooks. 2006. Complex multivariate sexual selection on male acoustic signaling in a wild population of *Teleogryllus commodus*. The American Naturalist 167: E102–E116.
- Bidochka, M. J., and A. E. Hajek. 1998. A nonpermissive entomophthoralean fungal infection increases activation of insect prophenoloxidase. Journal of Invertebrate Pathology 72: 231–238.
- Bonduriansky, R., and S. F. Chenoweth. 2009. Intralocus sexual conflict. Trends in Ecology and Evolution 24: 280–288.
- Bonduriansky, R., A. Maklakov, F. Zajitschek, and R. Brooks. 2008. Sexual selection, sexual conflict and the evolution of ageing and life span. Functional Ecology 22: 443–453.
- Box, G. E. P., and N. R. Draper. 1987. Empirical model-building and response surfaces. Wiley & Sons, New York, USA.
- Brown, G. P., and R. Shine. 2002. Reproductive ecology of a tropical natricine snake, *Tropidonophis mairii* (Colubridae). Journal of Zoology 258: 63–72.
- Bunning, H., L. Bassett, C. Clowser, J. Rapkin, K. Jensen, C. M. House, C. R. Archer, et al.

- 2016. Dietary choice for a balanced nutrient intake increases the mean and reduces the variance in the reproductive performance of male and female cockroaches. Ecology and Evolution 6: 4711-4730.
- Bunning, H., J. Rapkin, L. Belcher, C. R. Archer, K. Jensen, and J. Hunt. 2015. Protein and carbohydrate intake influence sperm number and fertility in male cockroaches, but not sperm viability. Proceedings of the Royal Society B: Biological Sciences 282: 20142144.
- Canty, A., and B. Ripley. 2016. Bootstrap R (S-Plus) functions. R package version 1.3-18, https://CRAN.R-project.org/package=boot
- Chippindale, A. K., A. G. Gibbs, M. Sheik, K. J. Yee, M. Djawdan, T. J. Bradley, and M. R. Rose.

 1998. Resource acquisition and the evolution of stress resistance in *Drosophila*melanogaster. Evolution 52: 1342–1352.
- Cotter, S. C., S. J. Simpson, D. Raubenheimer, and K. Wilson. 2011. Macronutrient balance mediates trade-offs between immune function and life history traits. Functional Ecology 25: 186–198.
- del Castillo, E., J. Hunt, and J. Rapkin. 2016. OptimaRegion: Confidence Regions for Optima.

 R package version 0.2, https://CRAN.R-project.org/package=OptimaRegion
- Draper, N. R., and J. A. John. 1988. Response-surface designs for quantitative and qualitative variables. Technometrics 30: 423–428.
- Dudycha, J. L., and M. Lynch. 2005. Conserved ontogeny and allometric scaling of resource acquisition and allocation in the Daphniidae. Evolution 59: 565–576.
- Efron, B., and R. Tibshirani. 1998. The problem of regions. Annals of Statistics 26: 1687 1718.
- French, S. S., D. F. DeNardo, and M. C. Moore. 2007. Trade-Offs between the reproductive and immune systems: facultative responses to resources or obligate responses to reproduction? The American Naturalist 170: 79–89.
- Galicia, A., R. Cueva del Castillo, and J. Contreras-Garduño. 2014. Is sexual dimorphism in the immune response of *Gryllodes sigillatus* related to the quality of diet? ISRN Evolutionary Biology 2014: 1–6.
- Gershman, S. N., C. A. Barnett, A. M. Pettinger, C. B. Weddle, J. Hunt, and S. K. Sakaluk.

 2010a. Give 'til it hurts: trade-offs between immunity and male reproductive effort in the decorated cricket, *Gryllodes sigillatus*. Journal of Evolutionary Biology 23:

- 829-839.
- Gershman, S. N., C. A. Barnett, A. M. Pettinger, C. B. Weddle, J. Hunt, and S. K. Sakaluk. 2010b. Inbred decorated crickets exhibit higher measures of macroparasitic immunity than outbred individuals. Heredity 105: 282–289.
- González-Santoyo, I., and A. Córdoba-Aguilar. 2012. Phenoloxidase: a key component of the insect immune system. Entomologia Experimentalis et Applicata 142: 1–16.
- Götz, P. 1986. Encapsulation in arthropods. Pages 153–170 *in* M. Brehélin, ed. Immunity in invertebrates. Springer, Berlin, Germany.
- Green, P. J., and B. W. Silverman. 1994. Nonparametric regression and generalised linear models. Chapman Hall, London, UK.
- Hadfield, J. D. 2010. MCMC methods for multi-response generalized linear mixed models: the MCMCglmm R package. Journal of Statistical Software 33: 1–22.
- Hagen, H.-E., J. Grunewald, and P. J. Ham. 1994. Induction of the prophenoloxidase activating system of *Simulium* (Diptera: Simuliidae) following *Onchocerca* (Nematoda: Filarioidea) infection. Parasitology 109: 649–655.
- Harrison, S. J., D. Raubenheimer, S. J. Simpson, J. G. Godin, and S. M. Bertram. 2014.

 Towards a synthesis of frameworks in nutritional ecology: interacting effects of protein, carbohydrate and phosphorus on field cricket fitness. Proceedings of the Royal Society B: Biological Sciences 281: 20140539.
- Hastie, T., R. Tibshirani, and J. Friedman. 2001. The elements of statistical learning theory.

 Springer, New York, USA.
- Henson, S. M., and T. G. Hallam. 1995. Optimal feeding via constrained processes. Journal of Theoretical Biology 176: 33–37.
- Hill, K., and H. Kaplan. 1999. Life history traits in humans: theory and empirical studies.

 Annual Review of Anthropology 28: 397–430.
- Hiruma, K., and L. M. Riddiford. 1988. Granular phenoloxidase involved in cuticular melanization in the tobacco hornworm: regulation of its synthesis in the epidermis by juvenile hormone. Developmental Biology 130: 87–97.
- House, C. M., K. Jensen, J. Rapkin, S. Lane, K. Okada, D. J. Hosken, and J. Hunt. 2015.

 Macronutrient balance mediates the growth of sexually selected weapons but not genitalia in male broad-horned beetles. Functional Ecology 30: 769-779.
- Houslay, T. M., J. Hunt, M. C. Tinsley, and L. F. Bussière. 2015. Sex differences in the effects

- of juvenile and adult diet on age-dependent reproductive effort. Journal of Evolutionary Biology 28: 1067–79.
- Hunt, J., R. Brooks, M. D. Jennions, M. J. Smith, C. L. Bentsen, and L. F. Bussiere. 2004. High quality male field crickets invest heavily in sexual display but die young. Nature 432: 1024–1027.
- Jacot, A., H. Scheuber, B. Holzer, O. Otti, and M. W. G. Brinkhof. 2008. Diel variation in a dynamic sexual display and its association with female mate-searching behaviour. Proceedings of the Royal Society B: Biological Sciences 275: 579–585.
- Jensen, K., C. McClure, N. K. Priest, and J. Hunt. 2015. Sex-specific effects of protein and carbohydrate intake on reproduction but not lifespan in *Drosophila melanogaster*.

 Aging Cell 14: 605–615.
- Kalbe, M., C. Eizaguirre, I. Dankert, T. B. H. Reusch, R. D. Sommerfeld, K. M. Wegner, and M. Milinski. 2009. Lifetime reproductive success is maximized with optimal major histocompatibility complex diversity. Proceedings of the Royal Society of London B: Biological Sciences 276: 925–934.
- Karell, P., H. Pietiäinen, H. Siitari, and J. E. Brommer. 2007. A possible link between parasite defence and residual reproduction. Journal of Evolutionary Biology 20: 2248–2252.
- Kauermann, G., G. Claeskens, and J. D. Opsomer. 2012. Bootstrapping for penalized spline regression. Journal of Computational and Graphical Statistics 18: 126-146.
- Kavanagh, M. W. 1987. The efficiency of sound production in two cricket species,

 Gryllotalpa australis and Teleogryllus commodus (Orthoptera: Grylloidea). Journal of

 Experimental Biology 130: 107-119.
- Kelly, C. D. 2016. Effect of nutritional stress and sex on melanotic encapsulation rate in the sexually size dimorphic Cook Strait giant weta (*Deinacrida rugosa*). Canadian Journal of Zoology 94: 787-792.
- Kolluru, G. R., and G. F. Grether. 2005. The effects of resource availability on alternative mating tactics in guppies (*Poecilia reticulata*). Behavioral Ecology 16: 294–300.
- Korner, P., and P. Schmid-Hempel. 2004. In vivo dynamics of an immune response in the bumble bee *Bombus terrestris*. Journal of Invertebrate Pathology 87: 59–66.
- Lande, R., and S. J. Arnold. 1983. The Measurement of Selection on Correlated Characters. Evolution 37: 1210–1226.
- Lardner, B., and J. Loman. 2003. Growth or reproduction? Resource allocation by female

- frogs Rana temporaria. Oecologia 137: 541–546.
- Lee, K. P., J. S. Cory, K. Wilson, D. Raubenheimer, and S. J. Simpson. 2006. Flexible diet choice offsets protein costs of pathogen resistance in a caterpillar. Proceedings of the Royal Society of London B: Biological Sciences 273:823–829.
- Lee, K. P., S. J. Simpson, F. J. Clissold, R. Brooks, J. W. Ballard, P. W. Taylor, N. Soran, et al. 2008a. Lifespan and reproduction in *Drosophila*: New insights from nutritional geometry. Proceedings of the National Academy of Sciences USA 105: 2498–2503.
- Lee, K. P., S. J. Simpson, and K. Wilson. 2008b. Dietary protein-quality influences melanization and immune function in an insect. Functional Ecology 22: 1052–1061.
- Maklakov, A. A., S. J. Simpson, F. Zajitschek, M. D. Hall, J. Dessmann, F. Clissold, D. Raubenheimer, et al. 2008. Sex-specific fitness effects of nutrient intake on reproduction and lifespan. Current Biology 18: 1062–1066.
- McCallum, M. L., and S. E. Trauth. 2007. Physiological trade-offs between immunity and reproduction in the northern cricket frog (*Acris crepitans*). Herpetologica 63: 269 274.
- McNamara, K.B., E. van Lieshout, T. M. Jones, and L. W. Simmons. 2012. Age-dependent trade-offs between immunity and male, but not female, reproduction. *Journal of Animal Ecology* 82: 235-244.
- Medley, G. F. 2002. The epidemiological consequences of optimisation of the individual host immune response. Parasitology 125: S61–S70.
- Mills, S. C., A. Grapputo, I. Jokinen, E. Koskela, T. Mappes, T. A. Oksanen, and T. Poikonen.

 2009. Testosterone-mediated effects on fitness-related phenotypic traits and fitness.

 The American Naturalist 173:475–487.
- Moore, S. L., and K. Wilson. 2002. Parasites as a viability cost of sexual selection in natural populations of mammals. Science 297: 2015–2018.
- Moreno, J., Sanz, J. Merino, S. & Arriero, E. 2001. Daily energy expenditure and cell-mediated immunity in pied flycatchers while feeding nestlings: interaction with moult. *Oecologia* 129: 492-497.
- Nordling, D., M. Andersson, S. Zohari, and G. Lars. 1998. Reproductive effort reduces specific immune response and parasite resistance. Proceedings of the Royal Society o London B: Biological Sciences 265: 1291–1298.
- Nychka, D. W. 2000. Spatial-process estimates as smoothers. Pages 393-424 in M. G.

- Schimek, ed. Smoothing and regression: approaches, computation, and application. Wiley and Sons, New York, USA.
- Nychka, D.W., Furrer, R., Paige, J., and Sain S. 2015. Fields: tools for spatial data. http://doi.org/10.5065/D6W957CT, R package version 8.4-1, www.image.ucar.edu/fields
- Ourth, D. D., and H. E. Renis. 1993. Antiviral melanization reaction of *Heliothis virescens* hemolymph against DNA and RNA viruses in vitro. Comparative Biochemistry and Physiology Part B: Comparative Biochemistry 105: 719–723.
- Penry, D. L., and P. A. Jumars. 1990. Gut architecture, digestive constraints and feeding ecology of deposit-feeding and carnivorous polychaetes. Oecologia 82: 1–11.
- Peterson, J. J., S. Cahya, and E. del Castillo. 2002. A general approach to confidence regions for optimal factor levels of response surfaces. Biometrics 58: 422–431.
- Poulin, R. 1996. Sexual inequalities in helminth infections: a cost of being a male? The American Naturalist 147: 287–295.
- Povey, S., S. C. Cotter, S. J. Simpson, K. P. Lee, and K. Wilson. 2009. Can the protein costs of bacterial resistance be offset by altered feeding behaviour? Journal of Animal Ecology 78: 437–446.
- Rajpurohit, S., L. M. Peterson, A. J. Orr, A. J. Marlon, and A. G. Gibbs. 2016. An experimental evolution test of the relationship between melanism and desiccation survival in insects. PloS One 11: e0163414.
- Rapkin, J., K. Jensen, S. M. Lane, C. M. House, S. K. Sakaluk, and J. Hunt. 2016.

 Macronutrient intake regulates sexual conflict in decorated crickets. Journal of Evolutionary Biology 29: 395–406.
- Rapkin, J., Jensen, K., House, C.M., Sakaluk, S.K., Sakaluk, J.K. & Hunt, J. 2017. The complex interplay between macronutrient intake, cuticular hydrocarbon expression and mating success in male decorated crickets. Journal of Evolutionary Biology 30: 711-727.
- Reddiex, A. J., T. P. Gosden, R. Bonduriansky, and S. F. Chenoweth. 2013. Sex-specific fitness consequences of nutrient intake and the evolvability of diet preferences. The American Naturalist 182: 91–102.
- Restif, O., and W. Amos. 2010. The evolution of sex-specific immune defences. Proceedings of the Royal Society of London B: Biological Sciences 277: 2247–2255.
- Reznick, D. 1985. Costs of reproduction: an evaluation of the empirical evidence. Oikos 44:

- 257-267.
- Reznick, D., L. Nunney, and A. Tessier. 2000. Big houses, big cars, superfleas and the costs of reproduction. Trends in Ecology and Evolution 15: 421–425.
- Roff, D. A. 2002. Life history evolution. Sinauer Associates Sunderland.
- Roff, D. A., and D. J. Fairbairn. 2007. The evolution of trade-offs: where are we? Journal of Evolutionary Biology 20: 433–447.
- Rolff, J. 2002. Bateman's principle and immunity. Proceedings of the Royal Society of London B: Biological Sciences 269: 867–872.
- Sadd, B.M. & Siva-Jothy, M.T. 2006. Self-harm caused by an insect's innate immunity.

 Proceedings of the Royal Society of London B: Biological Sciences 273: 2571–2574.
- Sakaluk, S. K. 1987. Reproductive behaviour of the decorated cricket, *Gryllodes supplicans* (Orthoptera: Gryllidae) calling schedules, spatial distribution and mating. Behaviour 100: 202–225.
- Saul, S. J., and M. Sugumaran. 1989. o-Quinone/quinone methide isomerase: A novel enzyme preventing the destruction of self-matter by phenoloxidase-generated quinones during immune response in insects. FEBS letters 249: 155–158.
- Schuurs, A. and H. A. M. Verheul. 1990. Effects of gender and sex steroids on the immune response. Journal of Steroid Biochemistry 35: 157–172.
- Schwenke, R. A., B. P. Lazzaro, and M. F. Wolfner. 2016. Reproduction-immunity trade-offs in insects. Annual Reviews of Entomology 61: 239–256.
- Sheridan, L. A., R. Poulin, D. F. Ward, and M. Zuk. 2000. Sex differences in parasitic infections among arthropod hosts: is there a male bias? Oikos 88: 327–334.
- Simpson, S. J., and J. D. Abisgold. 1985. Compensation by locusts for changes in dietary nutrients: behavioural mechanisms. Physiological Entomology 10: 443–452.
- Simpson, S. J., and D. Raubenheimer. 2012. The nature of nutrition: a unifying framework from animal adaptation to human obesity. Princeton University Press, Princeton, NJ, USA.
- South, S. H., C. M. House, A. J. Moore, S. J. Simpson, and J. Hunt. 2011. Male cockroaches prefer a high carbohydrate diet that makes them more attractive to females: implications for the study of condition dependence. Evolution 65: 1594–1606.
- Stearns, S. C. 1992. The evolution of life histories. Oxford University Press, Oxford, UK.
- Stoehr, A. M., and H. Kokko. 2006. Sexual dimorphism in immunocompetence: what does

- life-history theory predict? Behavioral Ecology 17: 751–756.
- Trivers, R. 1972. Parental investment and sexual selection. Pages 136–179 *in* B. Campbell, ed. Sexual selection and the descent of man 1871-1971. Aldine Publishing Company, Chicago, IL, USA.
- Tsakas, S., and V. J. Marmaras. 2010. Insect immunity and its signalling: an overview. ISJ 7: 228–238.
- Van Noordwijk, A. J., and G. de Jong. 1986. Acquisition and allocation of resources: their influence on variation in life history tactics. The American Naturalist 128: 137–142.
- Wheeler, D. 1996. The role of nourishment in oogenesis. Annual Review of Entomology 41: 407–431.
- Woutersen, T., and J. C. Ham. 2013. Calculating confidence intervals for continuous and discontinuous functions of parameters. Centre for Microdata Methods and Practice, Institute for Fiscal Studies, London, UK.
- Yeh, A.B. and K. Singh. 1997. Balanced confidence regions based on Tukey's depth and the bootstrap. *Journal of the Royal Statistical Society: Series B (Statistical Methodology)* 59: 639-652.
- Yin, H., Q. Shi, M. Shakeel, J. Kuang, and J. Li. 2016. The environmental plasticity of diverse body color caused by extremely long photoperiods and high temperature in *Saccharosydne procerus* (Homoptera: Delphacidae). Frontiers in Physiology 7: 401.
- Ypma, J. 2014. nlopr: R interface to NLopt. R package version 1.0.4, https://CRAN.R-project.org/package=nloptr
- Zera, A. J., and L. G. Harshman. 2001. The physiology of life history trade-offs in animals.

 Annual Review of Ecology and Systematics 32:95–126.
- Zuk, M. 2009. The sicker sex. PLoS Pathology 5: e1000267.
- Zuk, M., and K. A. McKean. 1996. Sex differences in parasite infections: patterns and processes. International Journal for Parasitology 26: 1009–1024.
- Zuk, M., and A. M. Stoehr. 2002. Immune defense and host life history. The American Naturalist 160: s9–s22.

References from the Appendices

- Mathai, A.M. 1992. On Bilinear Forms in Normal Variables. Annuals of the Institute of Statistical Mathematics 44: 769-779.
- Wolak, M.E., D. J. Fairbairn, and Y. R. Paulsen. 2012. Guidelines for estimating repeatability.

 Methods in Ecology and Evolution 3: 129–137.

Table 1. The linear and nonlinear effects of protein (P) and carbohydrate (C) intake on early life reproductive effort (calling effort and egg production) and immune function (encapsulation, inactive phenoloxidase activity and activated phenoloxidase activity) in male and female *Gryllodes sigillatus*.

	Linear effects			Nonlinear effects				
Response variable	Р	С		PxP	CxC	PxC		
Male								
Calling effort								
Coefficient ± SE	-0.10 ± 0.05	0.43 ± 0.05		0.00 ± 0.05	-0.08 ± 0.03	-0.19 ± 0.07		
t ₃₅₉	2.11	9.00		0.05	2.74	2.54		
Р	0.04	0.0001		0.96	0.006	0.01		
Encapsulation ability								
Coefficient ± SE	0.75 ± 0.04	-0.05 ± 0.04		-0.10 ± 0.03	0.02 ± 0.02	-0.36 ± 0.05		
t ₃₅₉	21.71	1.52		3.00	0.93	7.21		
Р	0.0001	0.31		0.003	0.35	0.0001		
Inactive phenoloxidase								
Coefficient ± SE	-0.07 ± 0.05	0.05 ± 0.05		0.06 ± 0.05	-0.04 ± 0.03	-0.10 ± 0.08		
t ₃₅₉	1.35	0.99		1.20	1.37	1.21		
Р	0.18	0.32		0.23	0.17	0.23		
Activated phenoloxidase								
Coefficient ± SE	0.05 ± 0.05	-0.09 ± 0.05		-0.08 ± 0.05	-0.02 ± 0.03	-0.06 ± 0.08		
t ₃₅₉	0.95	1.77		1.55	0.49	0.70		
Р	0.35	0.08		0.12	0.63	0.49		
Female								
Egg production								
Coefficient ± SE	0.44 ± 0.04	0.48 ± 0.04		-0.69 ± 0.14	-0.57 ± 0.13	0.45 ± 0.09		
t ₃₅₉	10.18	11.14		4.96	4.49	4.74		
Р	0.0001	0.0001		0.0001	0.0001	0.0001		
Encapsulation								
Coefficient ± SE	0.24 ± 0.05	0.15 ± 0.05		-0.47 ± 0.18	-0.42 ± 0.16	0.20 ± 0.12		
t ₃₅₉	4.65	2.80		2.70	2.57	1.68		
Р	0.0001	0.005		0.007	0.011	0.09		
Inactive phenoloxidase								
Coefficient ± SE	-0.03 ± 0.05	0.03 ± 0.05		0.07 ± 0.18	0.05 ± 0.17	0.04 ± 0.13		
t ₃₅₉	0.59	0.47		0.38	0.28	0.28		
Р	0.56	0.64		0.71	0.78	0.78		
Activated phenoloxidase								
Coefficient ± SE	-0.07 ± 0.05	0.03 ± 0.05		-0.11 ± 0.19	-0.11 ± 0.17	0.02 ± 0.13		
t ₃₅₉	1.22	0.60		0.56	0.67	0.15		
P	0.22	0.55		0.58	0.51	0.88		

Table 2. Differential linear and nonlinear effects of protein and carbohydrate intake on male and female reproductive effort and encapsulation ability in *Gryllodes sigillatus*.

Model term	SS _R	SS _c	DF ₁	DF ₂	F	P
Male calling effort vs						
Linear	627.99	436.57	2	714	156.53	0.0001 ^A
Quadratic	430.09	424.18	2	710	4.94	0.007 ^B
Correlational	402.68	400.46	1	708	3.93	0.05
Female egg producti						
Linear	589.62	566.33	2	714	14.68	0.0001 ^c
Quadratic	529.85	528.71	2	710	0.77	0.46
Correlational	515.65	513.82	1	708	2.52	0.11
Male calling effort vs						
Linear	568.20	517.05	2	714	35.31	0.0001 ^D
Quadratic	504.95	484.08	2	710	15.30	0.0001 ^E
Correlational	484.08	466.81	1	708	26.20	0.0001
Male vs. female enca						
Linear	545.07	485.85	2	714	43.52	0.0001 ^F
Quadratic	477.70	468.81	2	710	6.73	0.0013 ^G
Correlational	461.25	447.47	1	708	21.79	0.0001

Univariate tests: ^A P: $F_{1,714} = 209.64$, P = 0.0001, C: $F_{1,714} = 66.85$, P = 0.0001; ^B P x P: $F_{1,710} = 3.87$, P = 0.05, C x C: $F_{1,710} = 5.93$, P = 0.02; ^C P: $F_{1,714} = 8.607$, P = 0.003, C: $F_{1,714} = 24.686$, P = 0.0001; ^D P: $F_{1,714} = 70.436$, P = 0.0001, C: $F_{1,714} = 0.634$, P = 0.426; ^E P: $F_{1,710} = 23.915$, P = 0.0001, C: $F_{1,710} = 7.791$, P = 0.005; ^F P: $F_{1,714} = 67.423$, P = 0.0001, C: $F_{1,714} = 10.103$, P = 0.002; ^G P: $F_{1,710} = 9.499$, P = 0.0001, C: $F_{1,710} = 3.802$, P = 0.023

Table 3. MANOVA) examining differences in the protein (P) and carbohydrate (C) intake by male and female *Gryllodes sigillatus* when given the choice between alternate diets. Univariate ANOVAs was used to determine how each of the nutrients contributed to the overall multivariate effect. As *G. sigillatus* is sexually size dimorphic, body weight was included as a covariate in both the multivariate and univariate models.

	MANOVA						
Model term	Pillai's Trace	F	df	Р			
Sex (A)	0.71	181.38	2,151	0.0001			
Diet Pair (B)	1.04	55.36	6,304	0.0001			
AxB	0.21	5.91	6,304	0.0001			
		ANOVA					
	Nutrient	F	df	Р			
Sex (A)	Р	199.66	1,152	0.0001			
	С	291.24	1,152	0.0001			
Diet Pair (B)	Р	60.86	3,152	0.0001			
	С	66.35	3,152	0.0001			
AxB	Р	5.13	3,152	0.002			
	С	3.87	3,152	0.011			

Figure Legends

Figure A1. The distribution of the 24 artificial diets used in our no-choice feeding trial (Experiment 1). The diets are distributed along 6 nutritional rails (solid, black lines), with 4 diets per rail that differ in total nutritional content. The diets that are on different nutrient rails but connected by the iso-caloric lines (dashed, black lines) have equal total nutrition (i.e. P+C). The 4 diets marked with red symbols represent those used in diet pairs in our choice experiment feeding trial (Experiment 2).

Figure B1. Relation between covariation of two traits and the expected squared distance between their optima for the case of two covariates.

Figure B2. Relation between covariation of two traits and the approximate cosine of the angle between their optima (left) and between covariation of two traits and the expected angle (right) between their optima for the case of two covariates.

Figure 1. A hypothetical example demonstrating a typical protocol within the geometric framework for nutrition to study nutrient effects on lifespan. (A) The geometric distribution of diets presented in nutrient space. This particular geometric distribution consists of 9 different nutritional rails, each with a different fixed ratio of nutrient A to nutrient B (moving left to right: 1:8, 1:5, 1:3, 1:2, 1:1, 2:1, 3:1, 5:1 and 8:1). There are four different diets (black dots) located along each nutritional rail that have the same nutrient ratio but increase in total nutrition (i.e. energy or caloric content) as they move away from the origin. Across different nutritional rails the four diets are arranged so that they are connected by iso-caloric lines (dashed lines). These iso-caloric lines connect diets that have different A:B ratios but the same total nutritional content (which represents the percentage of nutrient A and B in the diet). This hypothetical nutrient space therefore consists of 36 unique diets that differ in both the A:B ratio and in total nutrition. (B) The distribution of actual feeding data (small black dots) recorded from animals restricted to each of the 36 unique diets. The consumption of diet by each animal is precisely measured over a defined feeding period, and because the nutritional composition of the diets is known, this consumption of diet can be easily converted to an intake of nutrient A and B. As each animal is restricted to a single diet, they can only feed along the length of the nutritional rail by eating more or less of the diet (thereby ingesting more or less nutrients and energy). (C) An example of a nutritional landscape for lifespan. For each animal where the intake of nutrient A and B has been

measured, the researcher also measures lifespan. This enables lifespan to be superimposed on the nutrient intake data and the linear and nonlinear effects of nutrient intake on lifespan can be quantified statistically using response surface methodologies. The relationship between nutrient intake and lifespan can also be visualized using thin-plate splines to plot the nutritional landscape in contour view. In the hypothetical example provided, the nutritional landscape is provided in contour view where regions in red represent increased lifespan and regions in blue represent reduced lifespan. The peak in lifespan appears to be centred at 50mg of nutrient A and 125 mg of nutrient B, which represents an A:B ratio of 1:2.5. To test whether animals regulate their intake of nutrients optimally for maximal lifespan, a researcher can present animals with alternate pairs of diets differing in the ratio of A to B and total nutrition. A typical dietary choice design might pair diets 1 and 3 (diet pair 1), 1 and 4 (diet pair 2), 2 and 4 (diet pair 3) and 2 and 3 (diet pair 4) (red dots, panel A) and measure the consumption of both diets and the subsequent total intake of A and B over a predefined time period. The average intake of nutrient A and B across these diet pairs is referred to as the regulated intake point (RIP) and represents the point in nutrient space that individuals actively defend when given dietary choice. The RIP (white cross, panel C) can be mapped onto the nutritional landscape and its proximity to the peak used to determine whether dietary choice is optimal for lifespan or any other measured trait.

Figure 2. A hypothetical example illustrating how to quantify differences in the strength of nutritionally regulated trade-offs between two life-history traits. In each panel, the nutritional landscape of two competing life-history traits is provided in contour view where the darker shading represents an increased expression of the trait and light shading a decreased expression of the trait. The dashed black lines in each panel are the A:B nutritional rail that passes through the nutritional optimum for each trait. The pair of curved, solid black lines that connect the nutritional rails passing through the optima represents the angle (θ) between these rails, and the red dashed line represents the Euclidean distance (d) between the global maxima for each life-history trait. Panels A to C represent the case where the nutritional optima for both life-history traits occur at the same (or very similar) caloric intake. Consequently, both θ and d provide an accurate measure of how divergent the nutritional optima are for the two life-history traits and therefore the strength of the nutritionally regulated trade-off between these traits. In moving from panel

A to C, the nutritional optima for the two life-history traits move closer together (ending with overlap in panel C) and both θ and d get smaller indicating that the strength of the nutritionally regulated trade-off between these traits is getting weaker. Panel D represents the case where the nutritional optima for the two life-history traits are located at two different caloric intakes. Consequently, θ and d provide different measures of the extent of the nutritionally regulated trade-off between life-history traits. In this instance d provides a better estimate of the divergence between optima and the strength of the life-history trade-off than θ .

Figure 3. Nutritional landscapes illustrating the linear and nonlinear effects of protein and carbohydrate intake on (A) calling effort and (B) encapsulation ability in males, and on (C) egg production and (D) encapsulation ability in female *G. sigillatus*. On each landscape, high values of these traits are given in red and low values in blue. The open black circles represent the actual nutrient intake data for each cricket and the closed white circles represent the global maximum on each landscape.

Figure 4. The 95% confidence region (solid grey fill) for the global maximum (closed black circle) on each landscape for (A) calling effort and (B) encapsulation ability in males, and for (C) egg production and (D) encapsulation ability in female *G. sigillatus*. On each landscape, the regulated intake point (± SE) is provided as a black cross and the dashed black line represents the boundary of the data. The regulation of nutrient intake under dietary choice is considered optimal for a given trait if the regulated intake point overlaps the 95% confidence region for the global maximum.

Figure 5. The mean (\pm SE) absolute consumption of each diet in the four diet pairs by (A) female and (B) male *G. sigillatus*. Grey bars represent the consumption of the high carbohydrate diet in the pair, whereas white bars represent the consumption of the high protein diet in the pair. The actual P:C ratio of alternate diets in each pair are provided above each bar and the total nutrient content of each diet are provided within the bar. The asterisks above each diet pair represent a significant difference (tested using a paired t-test) in the consumption of diets at P < 0.05. For each diet pair, males and females consumed significantly more of the high carbohydrate diet than the high protein diet. The difference in protein (white bars) and carbohydrate (grey bars) consumption from that expected if (C) females and (D) males fed at random from the diets in a pair. The asterisks above each bar represent a significant deviation from a mean of zero (tested using an unpaired t-test) which

is expected under random feeding. For each diet pair, males and females consumed significantly more carbohydrates than expected by random feeding and less protein.

Figure 6. The mean (±SE) protein and carbohydrate intake of male (open squares) and female (open circles) *G. sigillatus* on each of the four diet pairs (labelled by number). The regulated intake point, calculated as the mean intake of nutrients across diet pairs is also presented for males (solid black square) and females (solid black circle) at a P:C ratio of 1:2.00 and 1:1.84, respectively. The red dashed lines and red solid lines represent the span of mean P and C intake between the four diet pairs within males and females, respectively. The dashed black lines represent the expected intake of nutrients at a P:C ratio of 1:8, 1:3

and 1:1 (left to right of figure), respectively.

Figure 1.

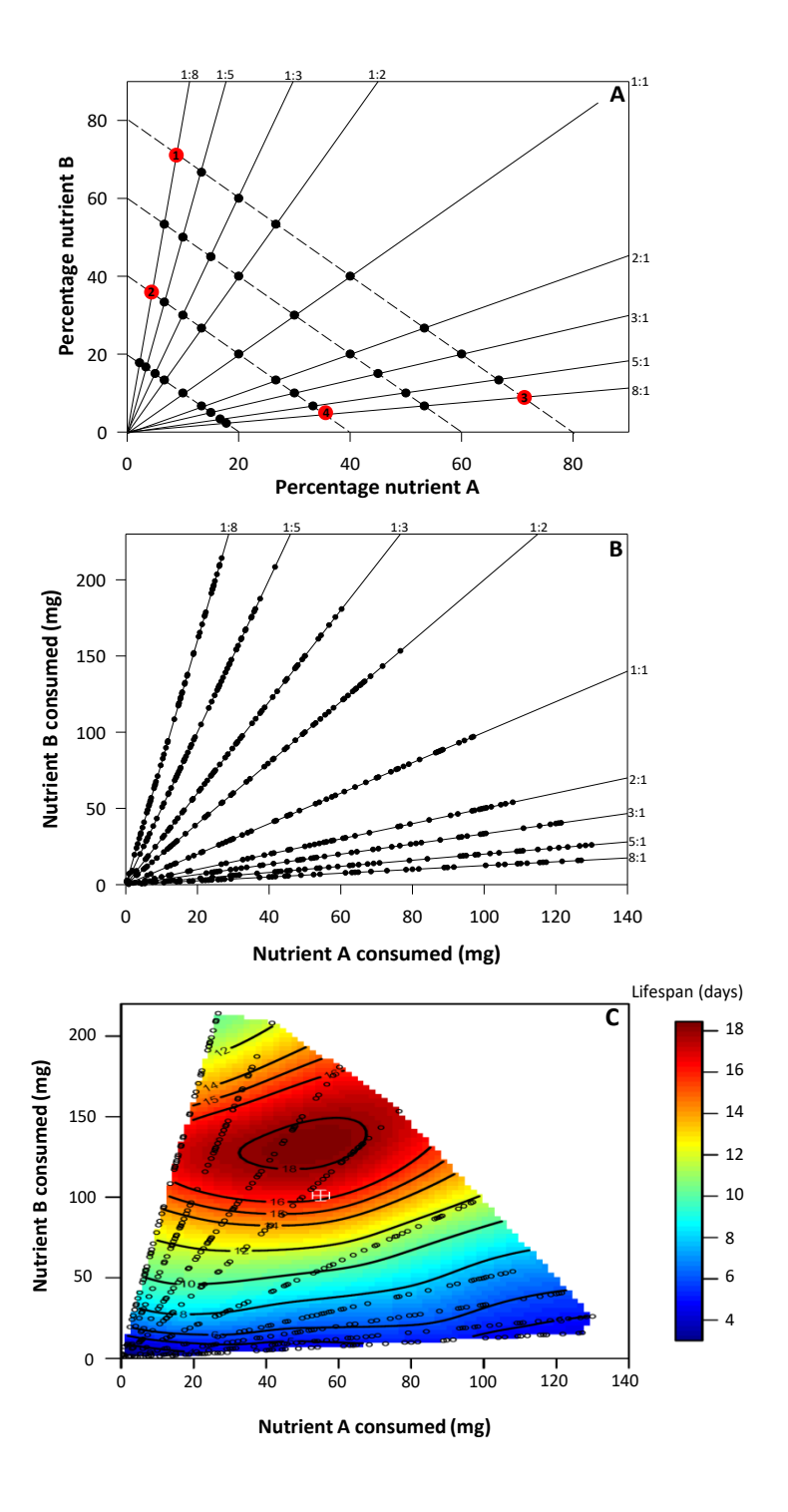
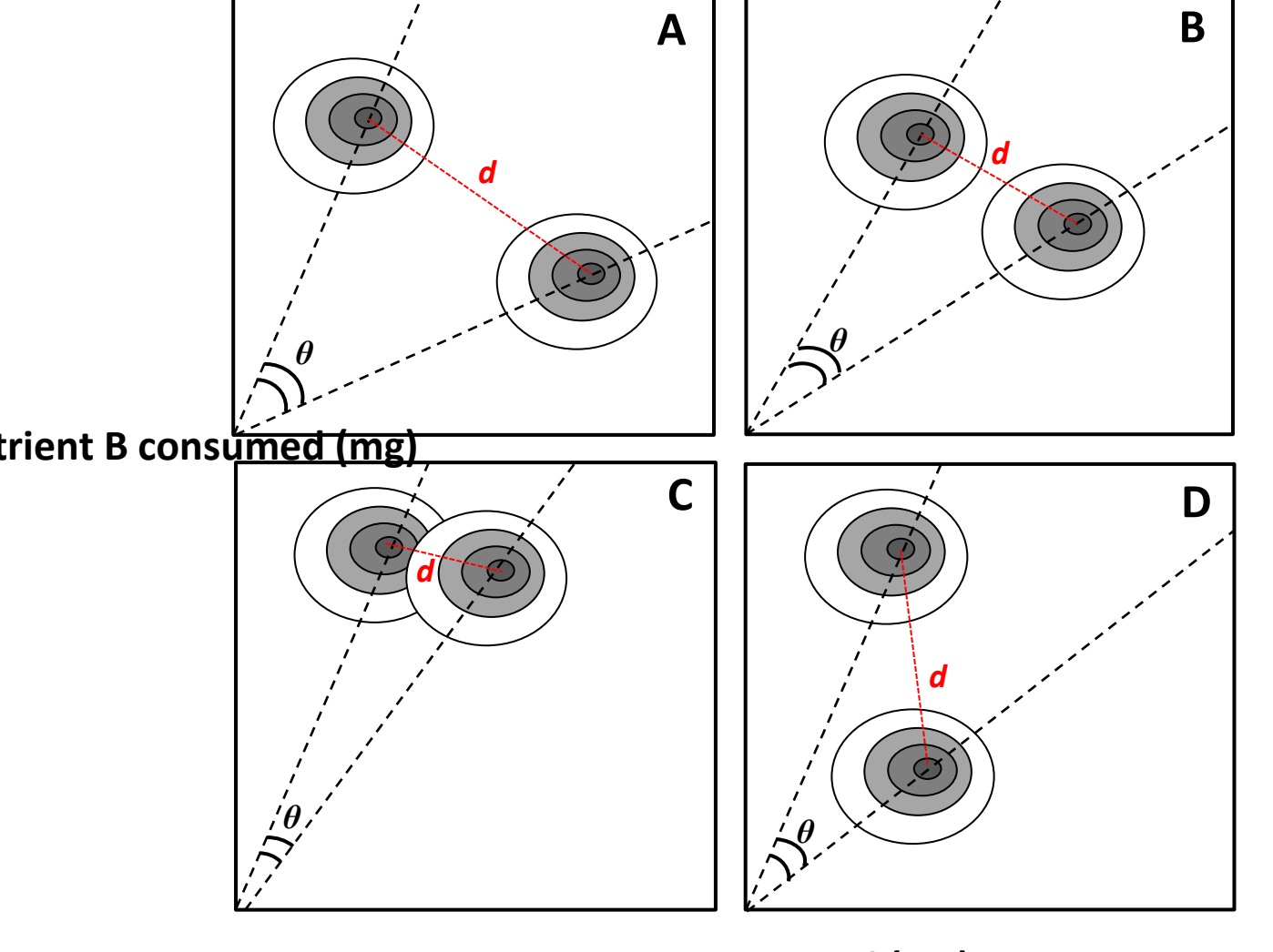


Figure 2.



Nutrient A consumed (mg)

Figure 3.

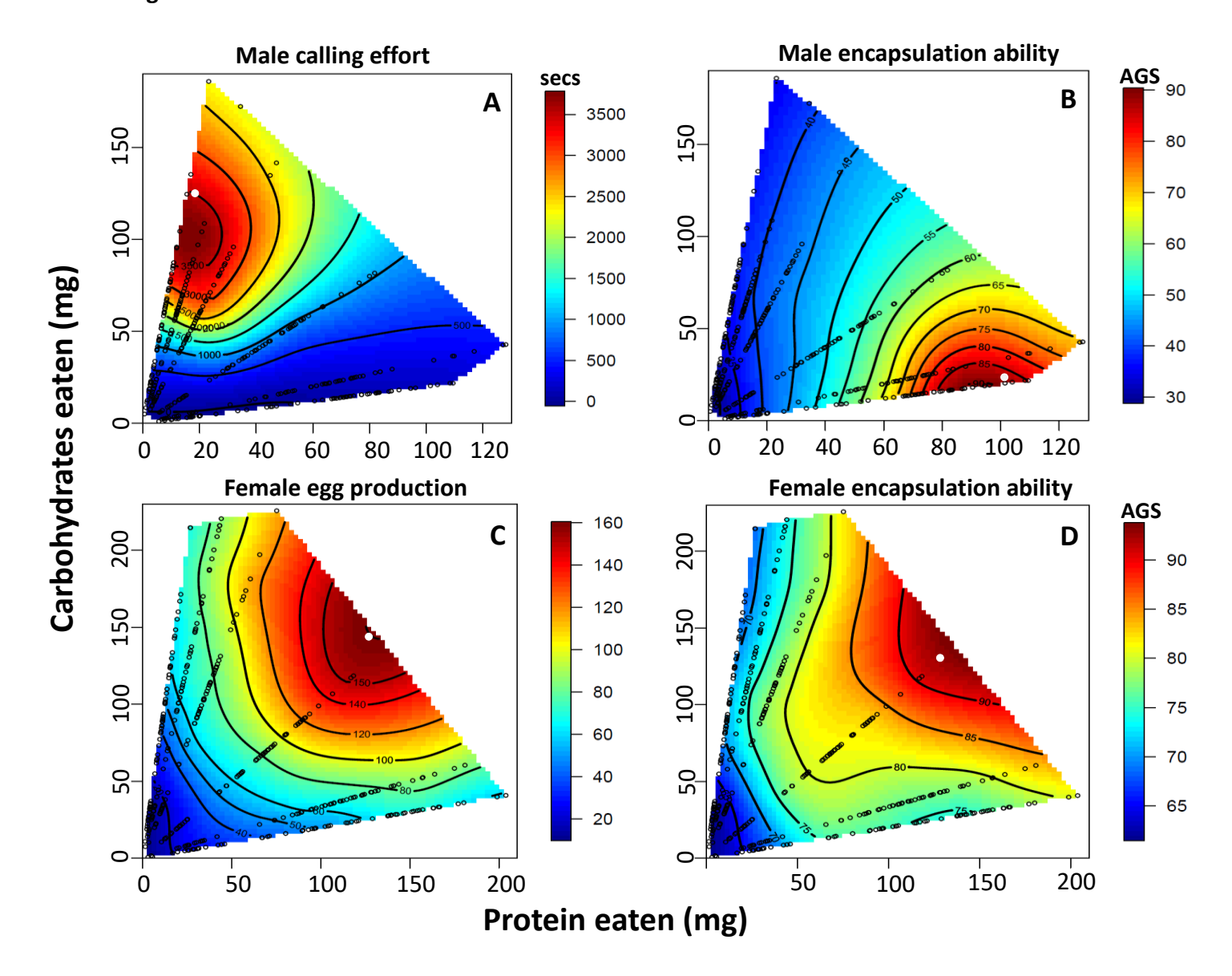


Figure 4.

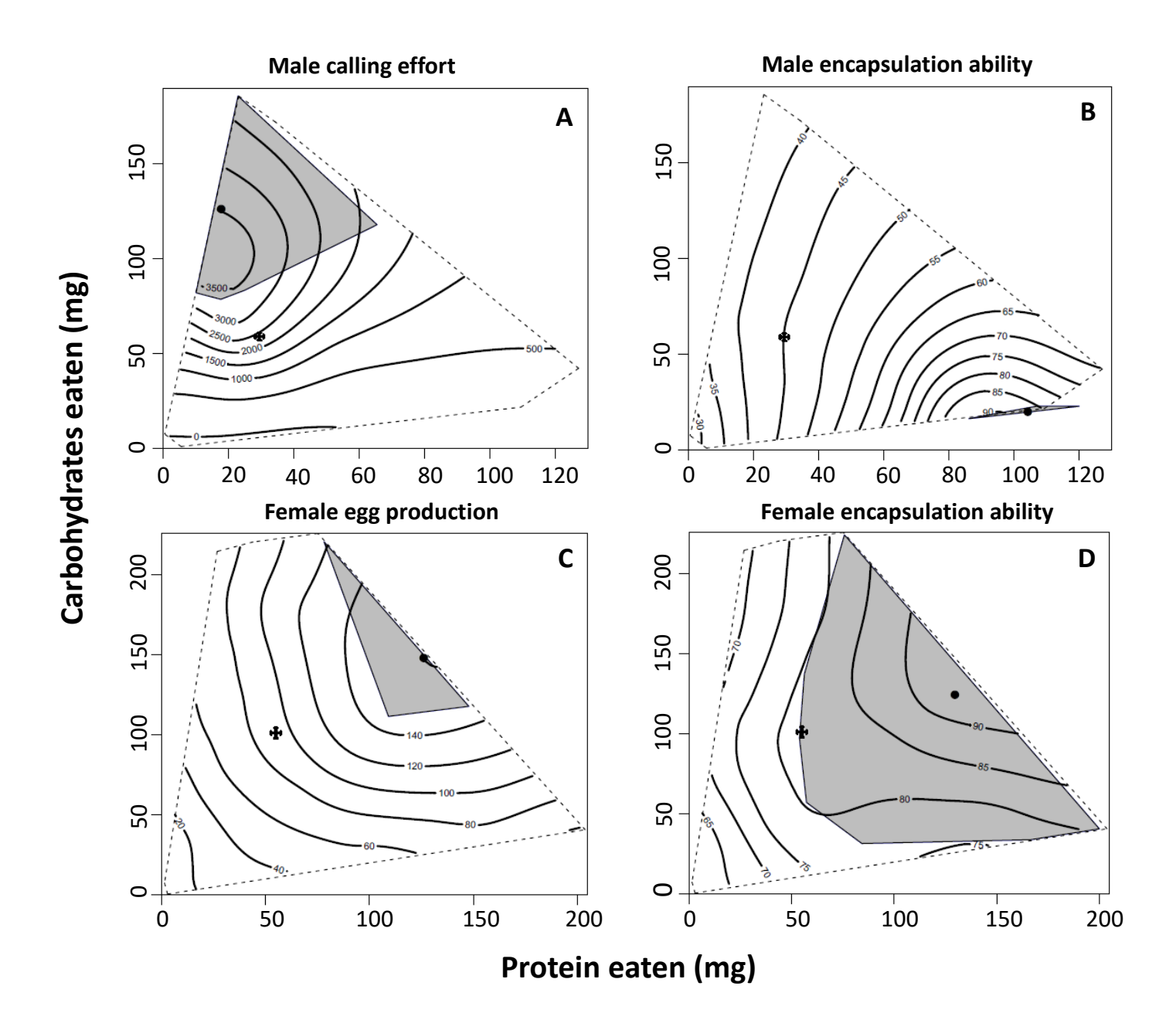


Figure 5.

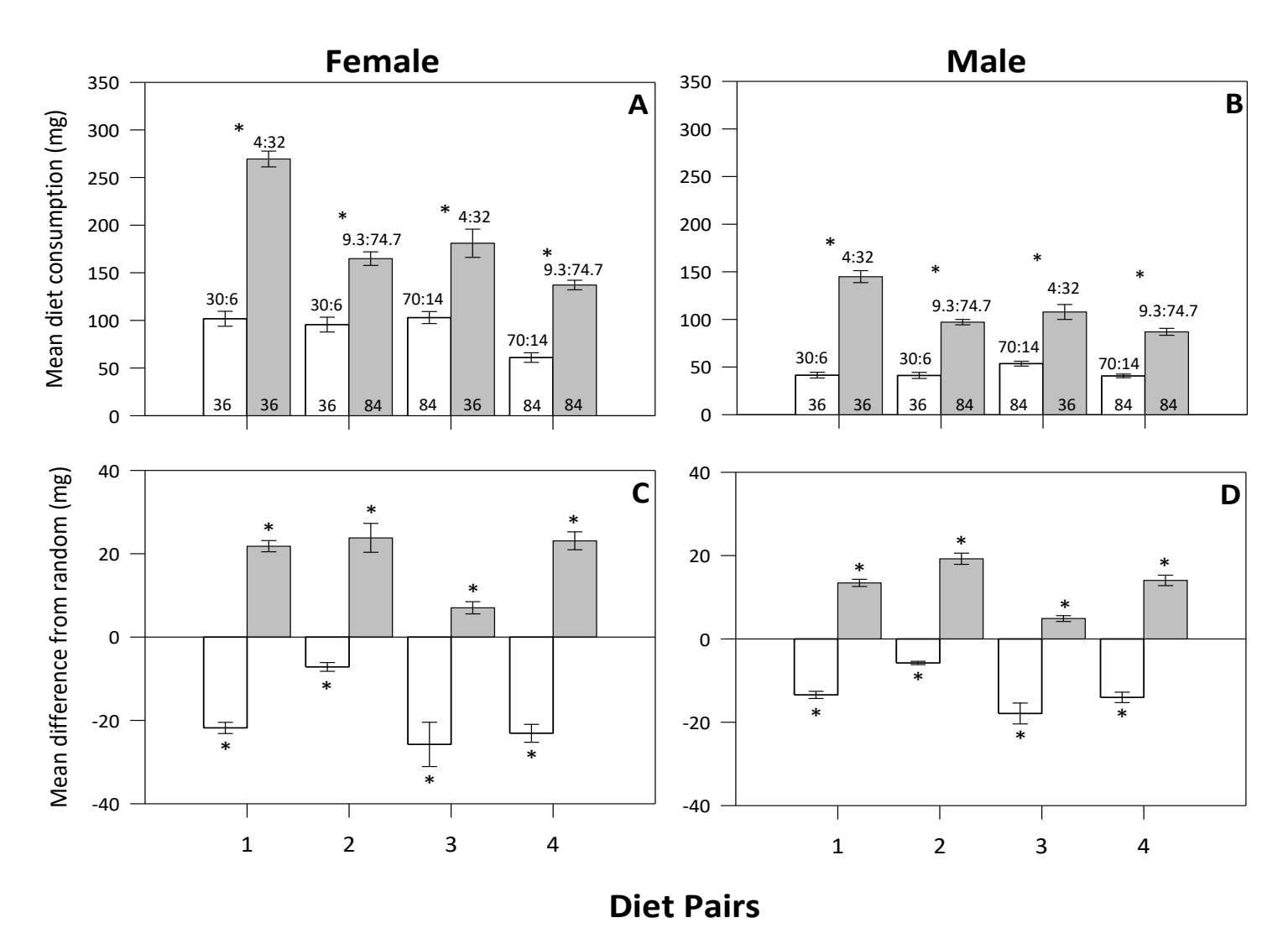


Figure 6.

